iScience

CellPress
OPEN ACCESS

Article

Interdependence of neural network dysfunction and microglial alterations in Alzheimer's disease-related models

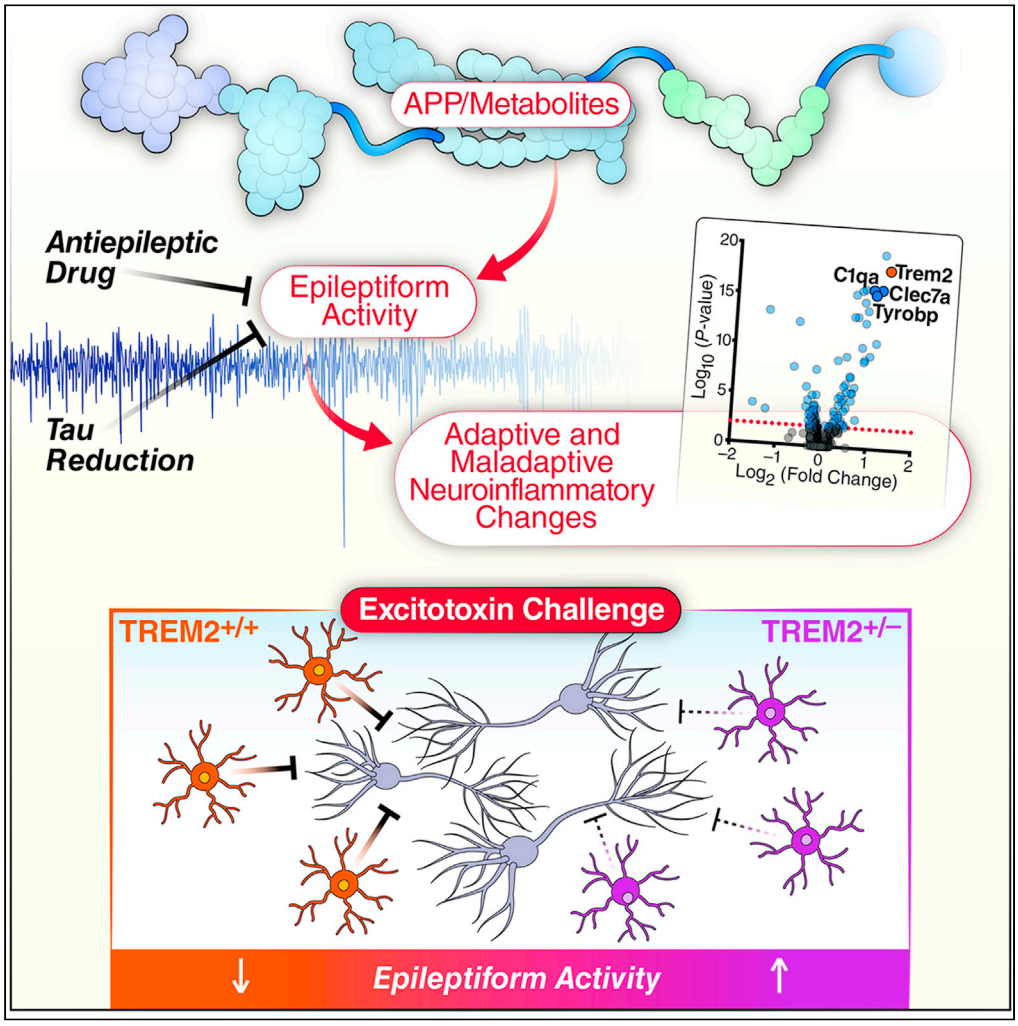

Melanie Das, Wenjie Mao, Eric Shao, ..., Xin Wang, Jiaming Wang, Lennart Mucke

lennart.mucke@gladstone.ucsf.edu

Highlights

Epileptiform activity and microglial mRNA changes in aged hAPP mice

Antiepileptic drug treatment and tau ablation reduce both abnormalities

TREM2 reduction exacerbates epileptiform activity after excitotoxin challenge

Neural network and microglial dysfunctions could form a vicious circle in AD

Das et al., iScience *24*, 103245
November 19, 2021
https://doi.org/10.1016/j.isci.2021.103245

iScience

CellPress
OPEN ACCESS

Article

Interdependence of neural network dysfunction and microglial alterations in Alzheimer's disease-related models

Melanie Das,[1] Wenjie Mao,[1] Eric Shao,[1] Soniya Tamhankar,[1] Gui-Qiu Yu,[1] Xinxing Yu,[1] Kaitlyn Ho,[1] Xin Wang,[1] Jiaming Wang,[1] and Lennart Mucke[1,2,3,*]

SUMMARY

Nonconvulsive epileptiform activity and microglial alterations have been detected in people with Alzheimer's disease (AD) and related mouse models. However, the relationship between these abnormalities remains to be elucidated. We suppressed epileptiform activity by treatment with the antiepileptic drug levetiracetam or by genetic ablation of tau and found that these interventions reversed or prevented aberrant microglial gene expression in brain tissues of aged human amyloid precursor protein transgenic mice, which simulate several key aspects of AD. The most robustly modulated genes included multiple factors previously implicated in AD pathogenesis, including TREM2, the hypofunction of which increases disease risk. Genetic reduction of TREM2 exacerbated epileptiform activity after mice were injected with kainate. We conclude that AD-related epileptiform activity markedly changes the molecular profile of microglia, inducing both maladaptive and adaptive alterations in their activities. Increased expression of TREM2 seems to support microglial activities that counteract this type of network dysfunction.

INTRODUCTION

Alzheimer's disease (AD), the most prevalent and costly neurodegenerative disorder (Wimo et al., 2017; El-Hayek et al., 2019; GBD 2016 Dementia Collaborators, 2019; Alzheimer's Association, 2020), is associated with diverse forms of neural network dysfunction, including non-convulsive epileptiform activity (Vossel et al., 2013, 2016; Palop and Mucke, 2016; Horváth et al., 2017; Lam et al., 2017, 2020; Lam and Noebels, 2020). However, the causes and consequences of AD-associated network dysfunctions remain to be fully elucidated. Evidence obtained in AD-related mouse models suggests that the human amyloid precursor protein (hAPP) or some of its metabolites and the microtubule-associated protein tau (MAPT) causally contribute to these dysfunctions (Palop and Mucke, 2016; Harris et al., 2020; Johnson et al., 2020; Chang et al., 2021; Hector and Brouillette, 2021). Indications that hypersynchronous network activity may promote disease progression include the observations that cognitive decline is faster in AD patients with detectable epileptiform activity than those without (Vossel et al., 2016), that treatment with the antiepileptic drug levetiracetam (LEV) reverses functional magnetic resonance imaging abnormalities and reduces some cognitive deficits in people with amnestic mild cognitive impairment (Bakker et al., 2012, 2015), and that treatment with LEV, or its analog brivaracetam, suppresses epileptiform activity and reverses both synaptic deficits and cognitive impairments in different lines of hAPP transgenic mice (Sanchez et al., 2012; Shi et al., 2013; Nygaard et al., 2015; Fu et al., 2019). hAPP mice also simulate multiple other features of AD, including pathologically elevated levels of amyloid-β (Aβ) peptides, amyloid plaques, dystrophic neurites, astrogliosis, and microgliosis (Palop and Mucke, 2016; Johnson et al., 2020). The molecular and cellular mechanisms that link neural network dysfunctions to other AD-relevant alterations and pathogenic processes have yet to be defined.

Independent lines of evidence have implicated myeloid cells and microglial dysfunction in the pathogenesis of AD, but the roles of microglia in AD have been studied primarily in relation to genetic risk factors and pathological hallmarks such as amyloid plaques and neurofibrillary tangles (Meyer-Luehmann and Prinz, 2015; Efthymiou and Goate, 2017; Sarlus and Heneka, 2017; Hammond et al., 2019; Leng and Edison, 2021). For example, variants of the triggering receptor expressed on myeloid cells 2 (TREM2) markedly

[1]Gladstone Institute of Neurological Disease, Gladstone Institutes, San Francisco, CA 94158, USA

[2]Department of Neurology and Weill Institute for Neurosciences, University of California, San Francisco, San Francisco, CA 94158, USA

[3]Lead contact

*Correspondence: lennart.mucke@gladstone.ucsf.edu

https://doi.org/10.1016/j.isci.2021.103245

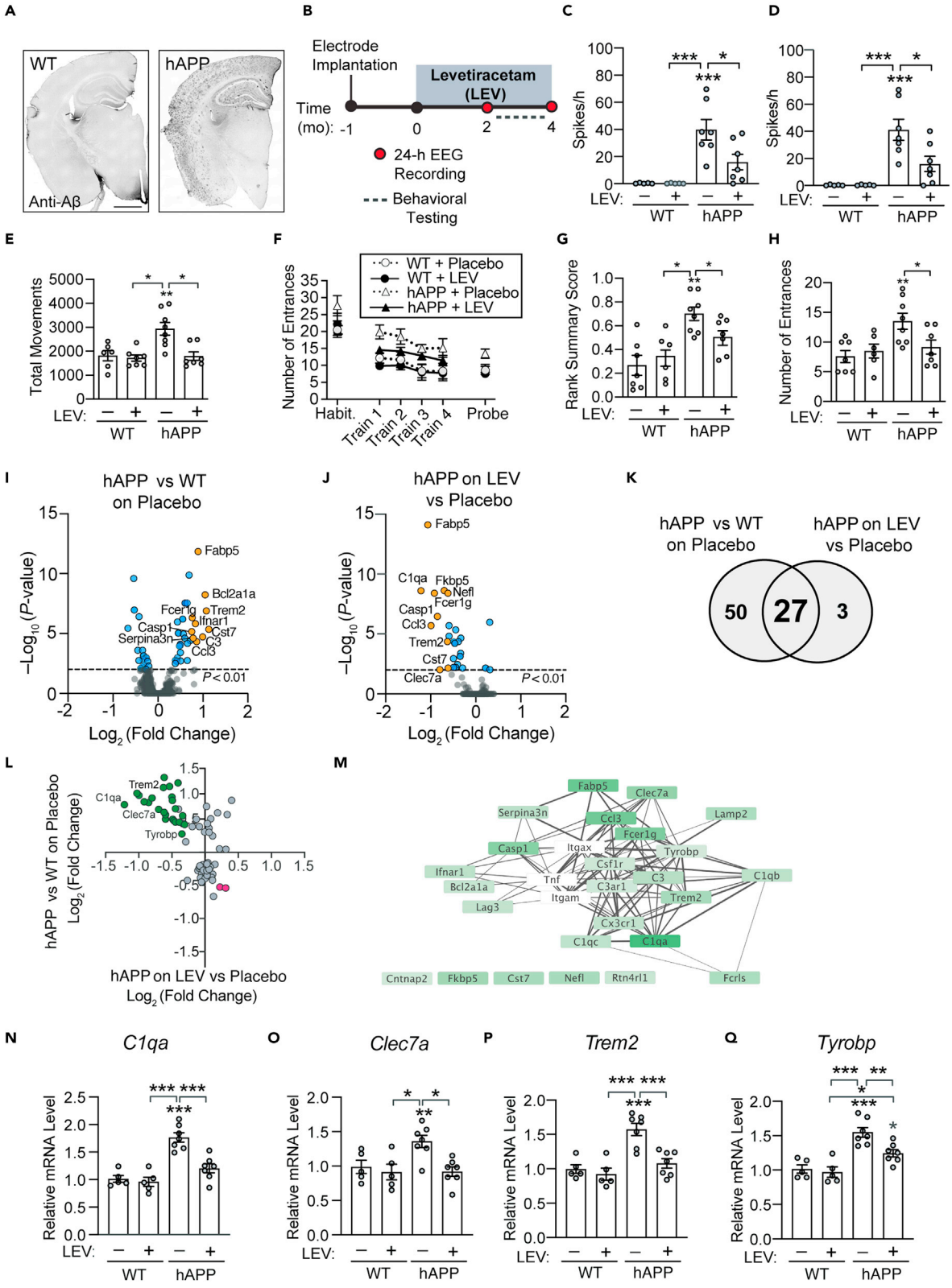
A
WT
hAPP
Anti-Aβ
B
Electrode Implantation
Levetiracetam (LEV)
Time (mo): -1 0 2 4
24-h EEG Recording
Behavioral Testing
C
Spikes/h
LEV:
WT
hAPP
D
Spikes/h
LEV:
WT
hAPP
E
Total Movements
LEV:
WT
hAPP
F
WT + Placebo
WT + LEV
hAPP + Placebo
hAPP + LEV
Number of Entrances
Habit.
Train 1
Train 2
Train 3
Train 4
Probe
G
Rank Summary Score
LEV:
WT
hAPP
H
Number of Entrances
LEV:
WT
hAPP
I
hAPP vs WT on Placebo
−Log10 (P-value)
Log2 (Fold Change)
P< 0.01
Fabp5
Bcl2a1a
Fcer1g
Trem2
Ifnar1
Casp1
Cst7
Serpina3n
C3
Ccl3
J
hAPP on LEV vs Placebo
−Log10 (P-value)
Log2 (Fold Change)
P< 0.01
Fabp5
C1qa
Fkbp5
Nefl
Fcer1g
Casp1
Ccl3
Trem2
Cst7
Clec7a
K
hAPP vs WT on Placebo
hAPP on LEV vs Placebo
50
27
3
L
hAPP vs WT on Placebo Log2 (Fold Change)
hAPP on LEV vs Placebo Log2 (Fold Change)
Trem2
C1qa
Clec7a
Tyrobp
M
Fabp5
Clec7a
Serpina3n
Ccl3
Lamp2
Fcer1g
Casp1
Itgax
Tyrobp
Ifnar1
Csf1r
C3
C1qb
Tnf
Bcl2a1a
C3ar1
Itgam
Trem2
Lag3
Cx3cr1
C1qc
C1qa
Cntnap2
Fkbp5
Cst7
Nefl
Rtn4rl1
Fcrls
N
C1qa
Relative mRNA Level
LEV:
WT
hAPP
O
Clec7a
Relative mRNA Level
LEV:
WT
hAPP
P
Trem2
Relative mRNA Level
LEV:
WT
hAPP
Q
Tyrobp
Relative mRNA Level
LEV:
WT
hAPP

Figure 1. LEV treatment reduces epileptiform activity, behavioral abnormalities and alterations in inflammation-related gene expression in aged, plaque-laden hAPP-J20 mice

(A) Coronal brain sections from 30-month-old mice of the indicated genotypes were labeled with an antibody against human Aβ (3D6). Scale bar: 500 μm. (B–Q) Intracranial EEGs were recorded on two occasions from 24–30-month-old male hAPP-J20 mice and WT controls while they were treated with levetiracetam (LEV) or placebo. After the second EEG recording, their hippocampal mRNA was analyzed with a NanoString Neuroinflammation panel and their cortical mRNA was analyzed by qRT-PCR. Behavioral testing was carried out in a replicate cohort of mice that were also treated with LEV or placebo but were not implanted with EEG electrodes. (B) Schematic of experiment. mo, months relative to beginning of LEV treatment. (C and D) Frequency of epileptiform spikes after 2 (C) or 4 (D) months of LEV (+; 2 g/kg of chow) or placebo (–) treatment. (E) Locomotor activity in the open field quantified as total movements per 10 min. (F–H) Learning and memory assessment in the active place avoidance (APA) paradigm. (F) Number of entries into the aversive zone during habituation (Habit., shock inactivated), training days 1–4 (shock activated), and a probe trial (shock inactivated). (G) Rank summary score of aversive zone entries during training. (H) Number of aversive zone entries during probe trial. (I and J) Volcano plots of transcripts whose levels differed in placebo-treated mice that did or did not express hAPP (I) and of transcripts whose levels differed in LEV- vs. placebo-treated hAPP-J20 mice (J). Transcripts with a p value < 0.01 are indicated in blue. Transcripts in orange and identified by name denote the ten genes with the largest $\log_2$ fold change and a p value < 0.01. (K) Venn diagram indicating the number of transcripts whose levels were significantly changed by one or both of the indicated experimental manipulations. (L) Log-fold change in expression for transcripts in (K). Transcripts whose levels were changed by both manipulations are highlighted in green or magenta. Transcripts in green and identified by name were selected for RT-qPCR analysis of cortical tissues from the same mice (N–Q). (M) STRING network analysis of proteins encoded by transcripts identified by green dots in (L). The darker the green, the greater the change LEV treatment caused in hAPP-J20 mice. Line thickness indicates the confidence score of the associations between nodes. Three additional proteins identified by STRING as potentially related to this network are shown in white boxes. Five proteins listed at the bottom left had no known associations with any of the other gene products. (N–Q) Cortical levels of the indicated transcripts were determined by qRT-PCR. Mean levels in placebo-treated mice without hAPP expression were defined as 1.0. n = 5–7 mice per group for (C, D, I, J, L, and N–Q) and 6–8 mice per group for (E–H). p values in (I and J) were obtained from a linear regression model followed by Benjamini–Yekutieli adjusted t-tests. Two-way ANOVA of the data in (C–H) revealed significant effects of genotype ($p < 0.05$) and treatment ($p < 0.05$), and a trend toward an interaction between them for (C, D; $p = 0.08$) but not (E–H; $p > 0.3$). Two-way ANOVA of the data in (N–Q) revealed significant effects of genotype (N–Q; $p < 0.001$) and treatment (N; $p < 0.05$ and P, Q; $p < 0.01$), and a significant interaction between these variables for some transcripts (N; $p < 0.05$; and P; $p < 0.01$) and a trend toward an interaction for another (O; $p = 0.06$). *$p < 0.05$, **$p < 0.01$, ***$p < 0.001$ by two-way ANOVA and Holm-Sidak test in (C–H, N–Q). Dots represent individual mice (C–H and N–Q) or transcripts (I, J, and L) and bars means ± s.e.m.

increase AD risk and have been shown to modulate both amyloid and tangle pathology in mouse models (Guerreiro et al., 2013; Jonsson et al., 2013; Gratuze et al., 2018; Ulland and Colonna, 2018). Other studies demonstrated that experimental enhancement of specific brain oscillations changes the morphology of microglia, expression of cytokines, and amyloid load in brain tissues of hAPP mice (Iaccarino et al., 2016; Martorell et al., 2019; Garza et al., 2020). However, it is unclear whether aberrant neural network activities that spontaneously arise in AD or related models alter microglial gene expression and whether preventing or reversing such neuronal dysfunctions can prevent or reverse altered immune responses in AD-relevant contexts. In the current study, we investigated the impact of non-convulsive epileptiform activity on the expression of microglial and other inflammation-related gene products in hAPP mice from line J20 (Mucke et al., 2000; Palop and Mucke, 2016; Johnson et al., 2020; Gulbranson et al., 2021) as well as the impact of TREM2 hypofunction on excitotoxin-induced network hypersynchrony.

RESULTS

LEV treatment suppresses neural network dysfunction and reverses inflammation-related gene expression changes in aged hAPP-J20 mice

It is widely thought that alterations in the expression of inflammation-related genes in brains of patients with AD and of related animal models are primarily caused by structural pathological alterations, particularly amyloid plaques and neurofibrillary tangles (Meyer-Luehmann and Prinz, 2015; Sarlus and Heneka, 2017; Gratuze et al., 2018; Leng and Edison, 2021). To determine whether functional alterations in neural network activities also contribute to gene expression changes by innate immune cells in AD-relevant contexts, we treated 22–26-month-old, plaque-laden (Figure 1A) male heterozygous hAPP-J20 mice and age/sex-matched, nontransgenic, wildtype (WT) controls from the same line with placebo or LEV for four months using chow formulations (Figure 1B). Intracranial EEG recordings at 2 and 4 months after treatment initiation revealed abnormally increased epileptiform activity in placebo-treated hAPP-J20 mice, as compared with placebo-treated WT controls (Figures 1C–1D). LEV treatment suppressed the epileptiform activity in hAPP-J20 mice, although it did not eliminate it completely at the dosage used here (Figures 1C–1D). Consistent with results obtained after treatment with LEV or the closely related drug brivaracetam in younger hAPP-J20 and APP/PS1 mice (Sanchez et al., 2012; Nygaard et al., 2015; Fu et al., 2019), LEV treatment reduced behavioral abnormalities in a replicate cohort of aged hAPP-J20 mice, including hyperactivity in the open field (Figure 1E) and spatial learning and memory deficits in the active place avoidance paradigm (Figures 1F–1H).

To identify altered immune responses, we used a NanoString Neuroinflammation panel to compare hippocampal mRNA levels in the four groups of mice that had undergone EEG recordings while they were treated with LEV or placebo. Compared with placebo-treated WT mice, more inflammation-related transcripts were increased than decreased in placebo-treated hAPP-J20 mice (Figure 1I; Table S1). LEV treatment changed the expression of multiple inflammation-related genes in hAPP-J20 mice (Figure 1J) and the majority of these changes reversed alterations that differentiated hAPP-J20 mice from WT controls (Figures 1K–1L).

To look for potential interactions among transcripts whose levels were altered by both hAPP expression and LEV treatment, we used STRING analysis (Szklarczyk et al., 2019). This approach provides information on direct (physical) and indirect (functional) associations derived from genomic context, co-expression data, text-mining, biochemical/genetic experiments, and previously curated pathway and protein-complex databases. Of the 25 gene products whose elevated levels in hAPP-J20 mice were reduced by LEV treatment, 20 showed interactions (Figure 1M). The majority of genes in this cluster are predominantly expressed in microglia and macrophages, and several are implicated in AD or related conditions. For example, the complement factor C1Q is found at abnormally high levels in brains of AD patients and hAPP mice; it is concentrated near amyloid plaques and colocalizes with synapses, possibly tagging them for elimination (Hong et al., 2016; Sarlus and Heneka, 2017; Hammond et al., 2019; Schartz and Tenner, 2020). C1Q levels are also elevated in epileptic conditions not associated with AD pathology (Schartz et al., 2018; Andoh et al., 2019). Expression of the pattern recognition receptor and immune response mediator CLEC7A is increased in microglia/macrophages in brains of hAPP mice (Keren-Shaul et al., 2017). Variants of TREM2 strongly increase AD risk (Guerreiro et al., 2013; Jonsson et al., 2013; Efthymiou and Goate, 2017). Levels of the TYRO protein tyrosine kinase-binding protein (TYROBP), an adaptor protein for TREM2, are increased in AD brains, and variants of TYROBP increase the risk for early-onset AD (Zhang et al., 2013; Pottier et al., 2016).

Quantitative RT-PCR (qRT-PCR) analysis revealed similar hAPP- and LEV-dependent modulations of these AD-relevant transcripts in the cortex of the mice whose hippocampal RNA we had analyzed with the NanoString Neuroinflammation panel (Figures 1N–1Q), demonstrating that the effects of our experimental manipulations are not restricted to one brain region. This set of data also illustrates how effectively LEV treatment counteracts the increased expression of these transcripts in hAPP-J20 mice, even though it does not affect their levels in WT controls (Figures 1N–1Q).

Some of the transcripts most strongly altered by both APP expression and LEV treatment were expressed predominantly by microglia/macrophages associated with amyloid plaques, as demonstrated by colabeling of coronal hemibrain sections from 26 to 30-month-old hAPP-J20 and WT mice with mRNA probes, antibodies against the cell-specific marker IBA1, and the amyloid stain Thioflavin S (ThioS) (Figure 2). In hAPP-J20 mice, *C1qa*, *Trem2*, and *Tyrobp* mRNA signals colocalized with IBA1-positive cells and the highest expression levels were seen around ThioS-positive plaques (Figures 2A–2C). None of the respective probes yielded detectable signals in WT mice (data not shown). Thus, at least some of the genes that were altered by hAPP and LEV treatment are expressed in microglia or infiltrating macrophages.

We also measured C1Q immunoreactivity in brain sections from hAPP-J20 and WT mice after LEV and placebo treatment to confirm that the changes we found in *C1qa*, *C1qb*, and *C1qc* transcript levels result in commensurate changes in C1Q protein levels. Compared to age-matched WT mice, C1Q immunoreactivity was increased within the hippocampus of hAPP-J20 mice, particularly in the molecular layer of the dentate gyrus and the *stratum lacunosum-moleculare* of the CA1–CA3 subfields (Figure S1). LEV treatment normalized hippocampal C1Q immunoreactivity levels in hAPP-J20 mice (Figure S1).

The most parsimonious interpretation of these results is that the microglia/macrophage-related gene expression changes that LEV treatment reduced in hAPP-J20 mice are caused, at least in good part, by epileptiform activity. The following experiments were designed to further test this hypothesis and to exclude alternative possibilities.

LEV treatment does not modulate amyloid plaques and plaque-associated microgliosis in aged hAPP-J20 mice or LPS-induced gene expression changes in other models

Previous studies demonstrated that treating 3-month-old hAPP-J20 mice with LEV or 13-month-old APP/PS1 mice with brivaracetam for 3–4 weeks did not alter Aβ levels or amyloid loads in their brain tissues

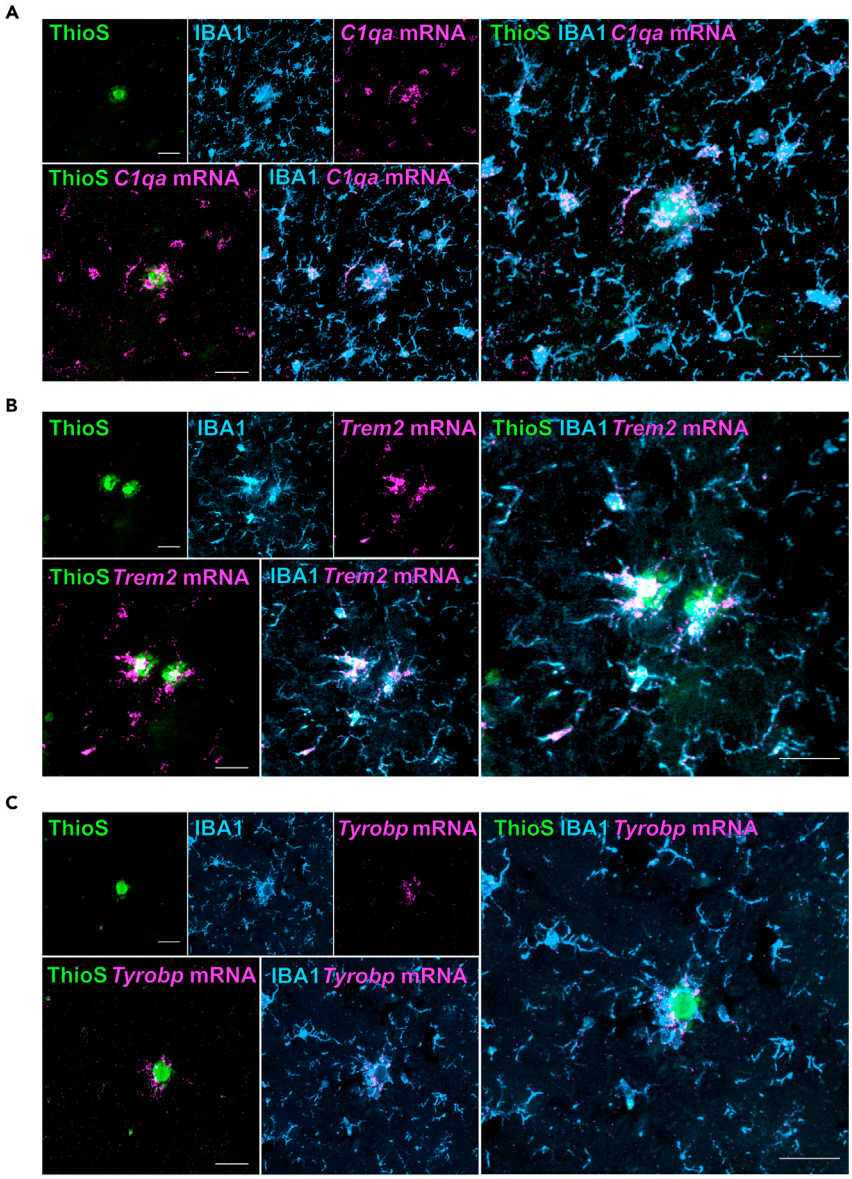

Figure 2. Transcripts modulated by hAPP expression and LEV treatment colocalize with IBA1-positive cells.
(A–C) Coronal brain sections from 26–30-month-old placebo-treated hAPP-J20 mice (Figure 1) were stained with ThioS (green), an IBA1 antibody (blue), and probes (magenta) against *C1qa* (A), *Trem2* (B), or *Tyrobp* (C) mRNA. Representative images are shown at different levels of magnification. Scale bars: 100 μm.

(Sanchez et al., 2012; Nygaard et al., 2015). To assess whether the more prolonged LEV treatment used here affected amyloid plaques and plaque-associated microgliosis in aged mice, we analyzed coronal hemibrain sections from 26–30-month-old hAPP-J20 mice after they had been treated for 4 months with LEV or placebo (Figure 1B). ThioS staining showed that both groups of mice had robust amyloid deposition in the hippocampus (Figure 3A). Quantitations of amyloid plaque numbers, plaque-associated ThioS signal intensities, plaque areas, and plaque circularities revealed no differences between LEV- and placebo-treated hAPP-J20 mice (Figures 3B–3E). In a similar vein, quantitative analyses of brain sections co-labeled with ThioS and an antibody against IBA1 revealed no differences between these groups of mice in regard to the number and morphology of microglia/macrophages associated with their plaques (Figures 3F–3I).

While the above findings make it unlikely that LEV treatment affects the expression of inflammation-related genes by changing plaques or the physical association between plaques and microglia, another possibility

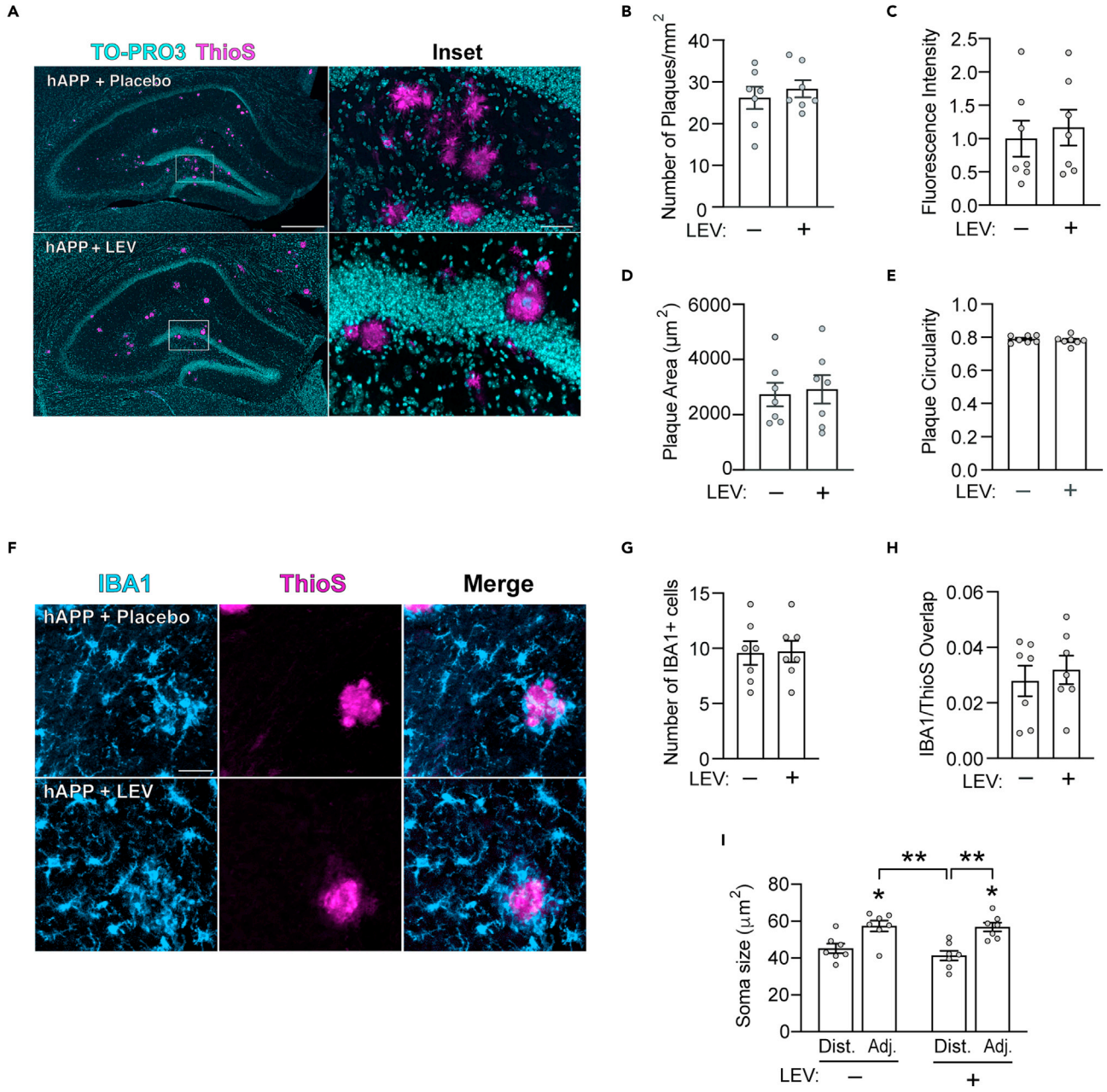

Figure 3. LEV does not alter amyloid plaque loads or plaque-associated microgliosis in hAPP-J20 mice

(A–I) Coronal brain sections from 26–30-month-old hAPP-J20 mice that had been treated with LEV or placebo (Figure 1) were stained with ThioS (magenta) to label plaques and with TO-PRO3 to label nuclei (cyan) (A–E) or with ThioS (magenta) and an IBA1 antibody to label microglia/macrophages (blue) (F–I). (A) Representative images of the hippocampus. Scale bars: 500 µm, 50 µm (inset). (B) Number of plaques per mm^2 of hippocampal area. (C) Fluorescence intensity of ThioS-positive plaques. Mean levels of fluorescence intensity in placebo-treated hAPP-J20 mice were defined as 1.0. (D) Area covered by ThioS positive plaques. (E) Plaque circularity. A perfect circle would equal 1.0. (F) Representative images of microglia/macrophages. Scale bar: 50 µm. (G) Number of IBA1-positive cell bodies within 25 µm of a ThioS-positive plaque. (H) Fraction of IBA1-positive pixels that were also positive for ThioS. (I) Soma size (area) of IBA1-postive cells that were located > 25 µm (distal, Dist.) or < 25 µm (adjacent, Adj.) of a ThioS-positive plaque. $n = 7$ mice per group (3 sections were analyzed per mouse) for (B–E and G–I). For (G–I), three plaques were analyzed in each section. For (I), three microglia distal to a plaque and three microglia adjacent to a plaque were analyzed. Unpaired, two-tailed Student's t-test of the data in (B–E and G–H) revealed no significant differences between groups. Two-way ANOVA of the data in (I) revealed an effect of distance to plaques ($p < 0.001$), but no significant effect of LEV treatment ($p = 0.41$) and no interaction between these variables ($p = 0.52$). *$p < 0.05$, **$p < 0.01$ vs. leftmost bar or as indicated by brackets by two-way ANOVA and Holm-Sidak test. Dots in (B–E and G–I) represent individual mice. Bars are means ± s.e.m.

to consider is that LEV might have direct effects on the expression of such genes. To explore whether LEV has immune-modulatory effects that are independent of its anti-epileptic activities, we activated the immune system *in vivo* by injecting 5–6-month-old male WT mice intraperitoneally (IP) with lipopolysaccharide (LPS), a manipulation that causes inflammatory responses throughout the body (Sousa et al., 2018), and *in vitro* by adding LPS to the medium of microglial cultures. In mice, LPS did not increase the frequency of epileptiform spikes (Figures S2A–S2B), but it robustly altered the expression of inflammation related genes in the cortex (Figures S2C–S2H). Some of the gene expression changes pointed in opposite directions from those observed in placebo-treated hAPP-J20 mice. For example, *C1qa* and *Trem2* transcript levels were decreased in LPS-treated WT mice (Figures S2C–S2D), consistent with previous findings (Sousa et al., 2018), but increased in placebo-treated hAPP-J20 mice (Figures 1N and 1P). Such differential responses are not surprising, as it is well established that microglia and macrophages react to distinct pathological challenges with differential changes in their molecular profiles (Flaris et al., 1993; Sousa et al., 2018). Most importantly, pre-treating mice with LEV did not change the LPS-induced alterations or affect the expression of inflammation-related genes in placebo-treated mice (Figures S2C–S2H).

LPS treatment also elicited robust gene expression changes in cultures of primary microglia from WT mice (Figures S2I–S2N). Treating the cultures with LEV over a range of doses did not modulate the LPS-induced changes or affect microglial gene expression under baseline (vehicle control) conditions (Figures S2I–S2N). Thus, LEV does not appear to directly affect microglial gene expression *in vivo* or *in vitro*.

Early LEV treatment or tau ablation suppresses neural network dysfunction and inflammation-related gene expression changes in hAPP-J20 mice

To assess the relationship among inflammation-related gene expression changes, epileptiform activity, and much earlier stages of amyloid deposition, we tested whether suppressing epileptiform activity could reverse inflammation-related gene expression changes in hAPP-J20 mice that were just beginning to form plaques in the hippocampus and had not yet formed plaques in the cortex ((Mucke et al., 2000; Sanchez et al., 2012; Fu et al., 2019; Whitesell et al., 2019) and data not shown). Starting at 6 months of age, hAPP-J20 mice and WT controls were treated with LEV or placebo for 1 or 3 months. Hippocampal and cortical levels of *C1qa*, *Trem2*, and *Tyrobp* mRNAs were determined by qRT-PCR at the end of the treatments. Compared with placebo-treated WT controls, increases in the expression of these transcripts were mostly seen in the hippocampus (Figure 4). At both ages, LEV treatment of either length reduced the increased expression of *C1qa*, *Trem2*, and *Tyrobp* mRNAs in hAPP-J20 mice but did not affect their levels in WT controls (Figure 4).

Next, we prevented the development of epileptiform activity in hAPP-J20 mice through the genetic ablation of endogenous mouse tau, a strategy that effectively counteracts network hypersynchrony in mouse models with epilepsy of diverse causes, including in hAPP-J20 mice (Roberson et al., 2007, 2011; Chang et al., 2021). EEG recordings in 22–26-month-old male and female $Mapt^{+/+}$ and $Mapt^{-/-}$ mice that did or did not express hAPP confirmed that hAPP-J20/$Mapt^{+/+}$ mice had an increased frequency of epileptiform spikes and that tau ablation prevented this abnormality in hAPP-J20/$Mapt^{-/-}$ mice (Figure 5A). Analysis of hippocampal mRNA from these mice by NanoString Neuroinflammation panel revealed that more inflammation-related transcripts were increased than decreased in hAPP-J20/$Mapt^{+/+}$ mice, as compared to WT controls, and that transcripts expressed predominantly in microglia and macrophages featured prominently among those that differed between these genotypes (Figure 5B; Table S2).

Tau ablation prevented 43 gene expression changes in hAPP-J20 mice, including increased expression of 28 and decreased expression of 15 transcripts (Figures 5C–5D;Table S2). In the absence of hAPP, tau ablation changed the expression of only one of the genes we investigated, *Mapt* (Table S2). To look for potential interactions among transcripts whose levels were altered by both hAPP and tau, we again used STRING analysis (Szklarczyk et al., 2019). Of the 28 gene products whose elevated levels in hAPP-J20 mice were reduced by tau ablation (Figures 5E), 25 showed interactions (Figure 5F). The majority of genes in this cluster are predominantly expressed in microglia and macrophages, and several have been implicated in AD or related conditions, similar to the cluster of genes whose aberrant expression in hAPP-J20 mice was reversed by LEV treatment (Figure 1M).

qRT-PCR analysis confirmed hAPP- and tau-dependent modulations of AD-relevant microglial transcripts in the cortex (Figures 5G–5J), again demonstrating that the effects of our experimental manipulations are

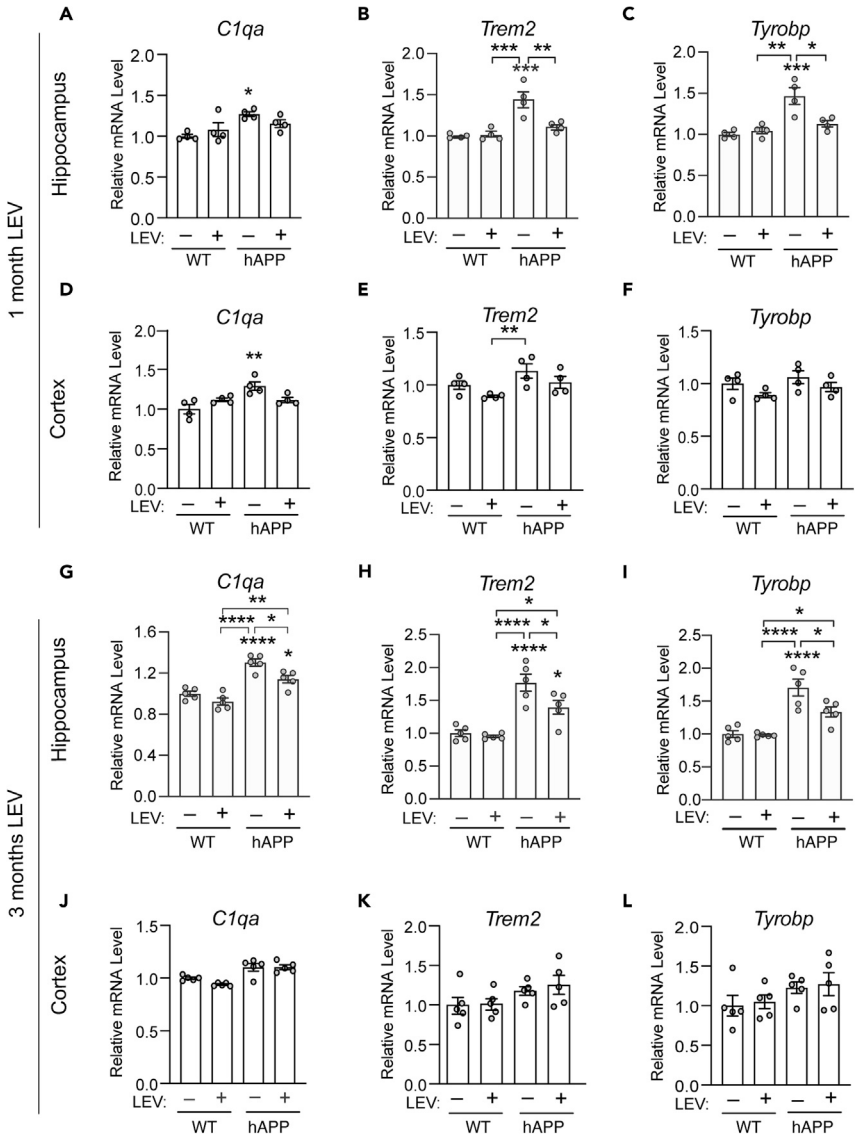

Figure 4. Effects of LEV treatment on microglial gene expression changes in young hAPP-J20 mice

(A–L) Male hAPP-J20 mice and WT controls were treated for 4 or 12 weeks with LEV (+; 2 g/kg of chow) or placebo (–) starting at 6 months of age. At the end of treatments, hippocampal and cortical mRNA was analyzed by qRT-PCR. (A–F) Hippocampal (A–C) and cortical (D–F) levels of the indicated transcripts after 4 weeks of LEV or placebo treatment. (G–L) Hippocampal (G–I) and cortical (J–L) levels of the indicated transcripts after 12 weeks of LEV or placebo treatment. Mean levels of the respective transcripts in placebo-treated mice without hAPP expression were defined as 1.0. n = 4–5 mice per group. *$p < 0.05$, **$p < 0.01$, ***$p < 0.001$, ****$p < 0.0001$ vs. leftmost bar or as indicated by brackets (two-way ANOVA and Holm-Sidak test). Two-way ANOVA revealed a significant effect of genotype on all transcripts but one (F, $p = 0.18$; E,K,L, $p < 0.05$; A,D, $p < 0.01$; C, $p < 0.001$; B,G,H,I,J, $p < 0.0001$), a significant effect of LEV treatment on some transcripts (B,E,H,I, $p < 0.05$; G, $p < 0.01$) but not others (A,C,D,F,J–L, $p > 0.05$), and a significant interaction between these variables for some transcripts (I, $p < 0.05$; D, $p < 0.01$) but not others (A–C,E–H,J–L, $p > 0.05$). Dots represent individual mice and bars means ± s.e.m.

not restricted to the hippocampus in aged mice. Tau ablation effectively prevented the increased expression of *C1qa*, *Clec7a*, *Trem2*, and *Tyrobp* mRNAs in hAPP-J20 mice but did not affect the levels of these transcripts in mice without hAPP expression (Figures 5G–5J). We previously demonstrated that tau ablation does not alter Aβ levels or the extent of amyloid pathology in brains of hAPP-J20 mice (Roberson et al., 2007). Thus, reduction of endogenous tau prevents epileptiform activity as well as aberrant gene expression by microglia/macrophages in the presence of pathologically elevated levels of hAPP/Aβ.

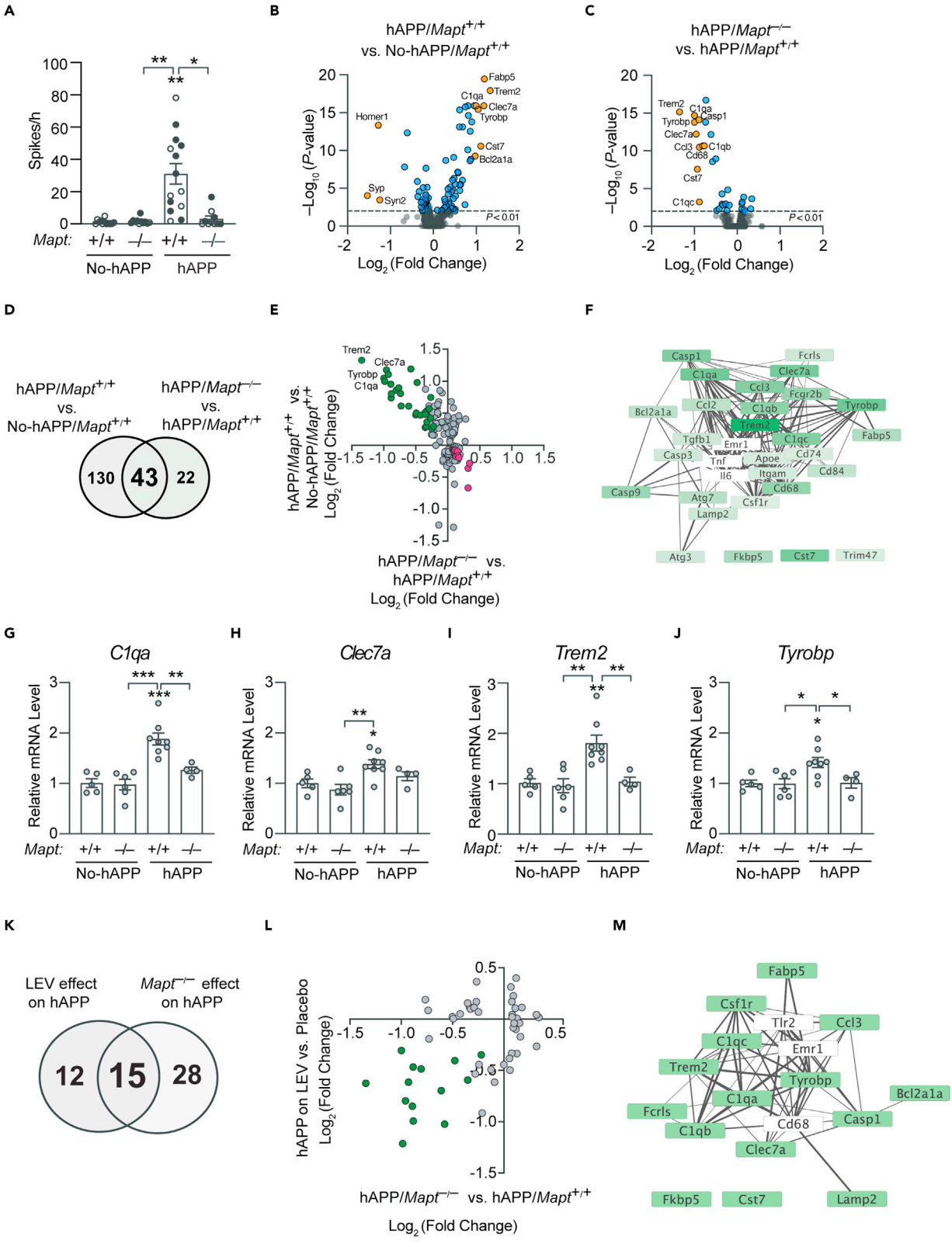
A
Spikes/h
Mapt: +/+ −/− +/+ −/−
No-hAPP
hAPP
B
hAPP/Mapt+/+ vs. No-hAPP/Mapt+/+
−Log10 (P-value)
Log2 (Fold Change)
P<0.01
C
hAPP/Mapt−/− vs. hAPP/Mapt+/+
D
hAPP/Mapt+/+ vs. No-hAPP/Mapt+/+
hAPP/Mapt−/− vs. hAPP/Mapt+/+
130
43
22
E
hAPP/Mapt−/− vs. hAPP/Mapt+/+ Log2 (Fold Change)
hAPP/Mapt+/+ vs. No-hAPP/Mapt+/+ Log2 (Fold Change)
F
G
C1qa
H
Clec7a
I
Trem2
J
Tyrobp
Relative mRNA Level
K
LEV effect on hAPP
Mapt−/− effect on hAPP
12
15
28
L
hAPP on LEV vs. Placebo Log2 (Fold Change)
hAPP/Mapt−/− vs. hAPP/Mapt+/+ Log2 (Fold Change)
M

Figure 5. Tau reduction prevents network dysfunction and microglial gene changes in aged hAPP-J20 mice

(A–J) EEG recordings were obtained from male and female *Mapt*$^{+/+}$ and *Mapt*$^{-/-}$ mice that did or did not express hAPP at 26–30 months of age. Hippocampal mRNA was analyzed with a NanoString Neuroinflammation panel. (A) Frequency of epileptiform spikes in male (black) and female (white) mice of the indicated genotypes. (B and C) Volcano plots of transcripts whose levels differed between *Mapt*$^{+/+}$ mice that did or did not express hAPP (B) and of transcripts whose levels differed between hAPP-J20 mice of the *Mapt*$^{-/-}$ vs. *Mapt*$^{+/+}$ background (C). Transcripts with a p value < 0.01 are indicated in blue. Transcripts in orange and identified by name denote the ten genes with the largest $\log_2$ fold change and a p value < 0.01. For (C), *Mapt* mRNA data was excluded before plotting to avoid disproportional scale expansion. (D) Venn diagram indicating the number of transcripts whose levels were significantly changed by one or both of the indicated genetic modifications. (E) Log-fold change in expression for transcripts in (D). Transcripts whose levels were changed by both manipulations are highlighted in green or magenta. Transcripts in green and identified by name were selected for RT-qPCR analysis of cortical tissues from the same mice (G–J). (F) STRING network analysis of proteins encoded by transcripts identified by green dots in (E). The darker the green, the greater the change tau ablation caused in hAPP-J20 mice. Line thickness indicates the confidence score of the associations between nodes. Three additional proteins identified by STRING as potentially related to this network are shown in white boxes. Three proteins listed at the bottom right had no known associations with any of the other gene products. (G–J) Cortical levels of the indicated transcripts were determined by RT-qPCR in the same mice whose hippocampi were analyzed with the NanoString Neuroinflammation panel (A–F). Mean levels of the respective transcripts in *Mapt*$^{+/+}$ mice without hAPP expression were defined as 1.0. (K–M) LEV treatment and tau reduction prevented or reversed an overlapping set of inflammation-related gene expression changes in hAPP-J20 mice. (K) Venn diagram indicating the number of transcripts whose hippocampal levels in 26–30-month-old hAPP-J20 mice were significantly changed by LEV treatment, tau ablation, or both (Figures 1 and 5A–5F). (L) Log-fold change in expression for transcripts in (K). Dots represent individual transcripts. Transcripts whose levels were changed by both manipulations are highlighted in green. (M) STRING network analysis of proteins encoded by transcripts identified by green dots in (L). Line thickness indicates the confidence score of the associations between nodes. Three additional proteins identified by STRING as potentially related to this network are shown in white boxes. Two proteins listed at the bottom left had no known associations with any of the other gene products. n = 10–14 (A–F), 4–8 (G–J), or 5–14 (K–M) mice per group. p values in (B and C) were obtained from a linear regression model adjusted for sex as a covariate followed by Benjamini–Yekutieli t-tests. Two-way ANOVA of the data in (A) revealed a significant effect of hAPP-J20 genotype ($p < 0.01$), a significant effect of *Mapt* genotype ($p < 0.01$), and a significant interaction between them ($p < 0.05$). Two-way ANOVA of the data in (G–J) revealed a significant effect of hAPP-J20 genotype (I,J, $p < 0.05$; G,H, $p < 0.01$), a significant effect of *Mapt* genotype for some transcripts (G,I, $p < 0.05$), a trend in this direction for others (H = 0.07, J = 0.06), and a significant interaction between these variables for some transcripts (G,I, $p < 0.05$) but not others (H = 0.57, J = 0.07). *$p < 0.05$, **$p < 0.01$, ***$p < 0.001$ vs. leftmost bar or as indicated by brackets by two-way ANOVA and Holm-Sidak test. Dots represent individual mice (A and G–J) transcripts (B, C, and E). Bars are means ± s.e.m.

Notably, several of the inflammation-related gene expression changes that were prevented by tau ablation in aged hAPP-J20 mice were also reversed by LEV treatment (Figures 5K–5M;Table S3). Furthermore, multiple gene expression changes correlated with the frequency of epileptiform spikes in untreated aged male and female hAPP-J20 mice and in placebo-treated aged male hAPP-J20 mice. Expression changes of 13 genes correlated with the frequency of epileptiform spikes in at least two of these groups (Figure 6A), and *Tyrobp* expression levels correlated with the frequency of epileptiform spikes in all three groups (Figures 6B–6D). Taken together, these results support the hypothesis that the effects of tau ablation on inflammation-related gene expression in hAPP-J20 mice resulted from the prevention of epileptiform activity.

Hypofunction of TREM2 enhances epileptiform activity

Although inflammatory changes, and microglial activities in particular, are often suspected of promoting the development of disease, the immune system clearly also fulfills many protective functions (Wyss-Coray and Mucke, 2002; Meyer-Luehmann and Prinz, 2015; Sarlus and Heneka, 2017; Schartz and Tenner, 2020; Leng and Edison, 2021). TREM2 is especially interesting in this regard, as its hypofunction seems to be a strong risk factor for AD (Guerreiro et al., 2013; Jonsson et al., 2013; Efthymiou and Goate, 2017; Ulland and Colonna, 2018) and its expression was robustly increased in hAPP-J20 mice and normalized by both LEV treatment (Figures 1I, 1J, 1L, 1P, 4B, and 4H) and tau ablation (Figures 5B, 5C, 5E, and 5I). We therefore wondered whether TREM2 has a role in microglial responses to neural network dysfunction.

To explore this possibility and simulate the hypofunction of TREM2 that is thought to increase AD risk in heterozygous carriers of certain TREM2 variants (Guerreiro et al., 2013; Jonsson et al., 2013; Efthymiou and Goate, 2017; Cheng-Hathaway et al., 2018; Sudom et al., 2018; Ulland and Colonna, 2018), we analyzed heterozygous *Trem2* knockout (*Trem2*$^{+/-}$) mice, whose TREM2 levels are reduced by 50%. To directly address whether hypofunction of TREM2 modulates epileptiform activity, we challenged *Trem2*$^{+/-}$ and WT mice with a subthreshold dose (10 mg/kg of body weight) of the proepileptic drug kainate, an approach that avoids confounding interactions between TREM2 and hAPP metabolites. Although we detected no difference in epileptiform activity between *Trem2*$^{+/-}$ mice and WT (*Trem2*$^{+/+}$) controls at baseline, Trem2$^{+/-}$ mice had more epileptiform activity than WT mice after the kainate challenge (Figures 7A–7C). Longitudinal analysis of EEG recordings revealed that after the kainate injection, peak spike frequencies were much higher and reached faster in *Trem2*$^{+/-}$ than *Trem2*$^{+/+}$ mice (Figures 7D–7F). The excitotoxin-induced epileptiform activity also took much longer to subside in *Trem2*$^{+/-}$ than *Trem2*$^{+/+}$ mice, resulting

A

Axl	AXL receptor tyrosine kinase
C1qc	Complement component 1, q subcomponent, C chain
Cd33	CD33 antigen
Cd74	CD74 antigen
Cd84	CD84 antigen
Fcgr1	Fc receptor, IgG, high affinity I
Gadd45a	Growth arrest and DNA-damage-inducible 45 alpha
Mpeg1	Macrophage expressed gene 1
Psmb8	Proteasome subunit, beta type 8
Rad9a	RAD9 checkpoint clamp component A
Smarca5	SWI/SNF related, matrix associated, actin dependent regulator of chromatin, subfamily a, member 5
Tyrobp	TYRO protein tyrosine kinase binding protein
Vps4b	Vacuolar protein sorting 4B
Kdm5c	Lysine (K)-specific demethylase 5C

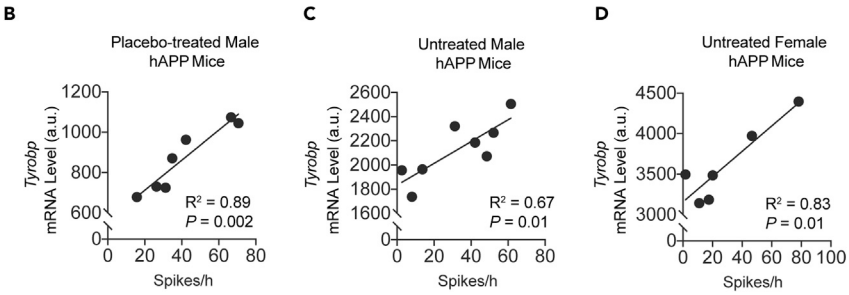

Figure 6. Microglial/macrophage gene expression changes correlate with the frequency of epileptiform spikes in hAPP-J20 mice

(A) List of genes whose expression levels correlated positively (white) or negatively (black) with the frequency of epileptiform spikes ($p < 0.05$ calculated from Pearson correlation coefficients) in at least two of the following groups of mice: placebo-treated male hAPP-J20 mice ($n = 7$) (Figure 1) or untreated male ($n = 8$) or female ($n = 6$) hAPP-J20 mice (Figures 5A–5J).

(B–D) Hippocampal *Tyrobp* mRNA levels correlated positively with the frequency of epileptiform spikes in placebo-treated male hAPP-J20 mice (B) and in untreated male (C) or female (D) hAPP-J20 mice. Pearson correlation coefficients (r) and p values are shown in the graphs. Dots represent individual mice.

in an increased overall burden of epileptiform spikes in *Trem2*$^{+/-}$ mice (Figures 7G–7I). Taken together, these findings suggest that the increased expression of TREM2 in hAPP-J20 mice represents an adaptive response, an important purpose of which may be to curtail hypersynchronous neural network activity.

DISCUSSION

The results from our investigation of hAPP-J20 mice suggest that the aberrant expression of inflammation-related genes in brains with pathologically elevated levels of hAPP/Aβ and extensive plaque loads are driven and mediated, at least in part, by epileptiform activity, a type of neural network dysfunction that also occurs in patients with AD (Vossel et al., 2013, 2016; Palop and Mucke, 2016; Horváth et al., 2017; Lam et al., 2017, 2020; Lam and Noebels, 2020). This conclusion is supported by our findings that these gene expression changes correlated with the extent of epileptiform activity and could be reduced by two distinct experimental interventions (LEV treatment and tau ablation) that suppress epileptiform activity in aged, plaque-laden hAPP-J20 mice. It is worth noting in this context that both LEV treatment (ClinicalTrials.gov number NCT03486938) and an antisense oligonucleotide strategy to reduce overall tau levels (ClinicalTrials.gov number NCT03186989) are currently undergoing clinical trials in patients with early stages of AD. To what extent the modulation of inflammation-related gene expression changes contributes to the reduction of synaptic deficits, cognitive impairments, and behavioral abnormalities that have been observed in hAPP mice after LEV or brivaracetam treatment (refs.(Sanchez et al., 2012; Nygaard et al., 2015; Fu et al., 2019) and current study) and after tau reduction (Roberson et al., 2007, 2011; Chang et al., 2021) remains to be determined. Additional studies are also needed to validate our findings in independent mouse models and the human condition and to expand them to the level of single cells.

Although LEV treatment and tau ablation markedly reduced inflammation-related gene expression changes in aged hAPP-J20 mice, it remains possible that these gene expression changes are not caused solely by epileptiform activity, but also depend on the presence of amyloid plaques, which could prime

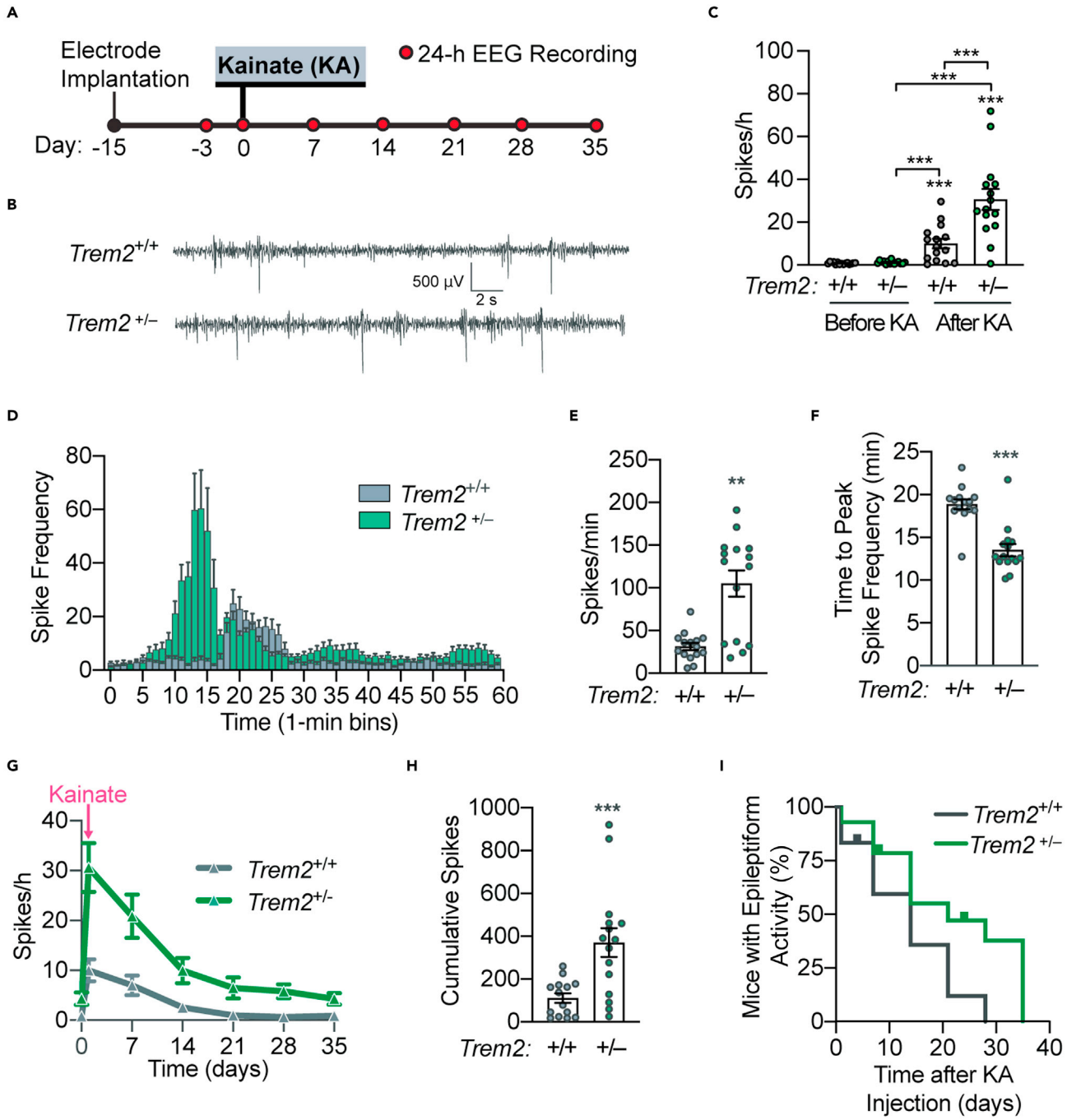

Figure 7. Genetic reduction of *Trem2* exacerbates epileptiform activity after low-dose kainate challenge

(A–I) EEG recordings were obtained from 6-month-old male *Trem2*$^{+/-}$ mice and WT (*Trem2*$^{+/+}$) controls before and after a single IP injection of kainate (10 mg/kg body weight). (A) Schematic of experiment. (B) Sample EEG traces during the first hour after kainate injection. (C) Spike frequency 24 h before and after kainate injection. (D) Number of spikes per min during the first hour after kainate injection. (E) Peak spike frequency after kainate injection. (F) Time to reach peak spike frequency after kainate injection. (G) Change in spike frequency over 35 days after kainate injection. (H) Cumulative spikes estimated by calculating the area under the curve in (G). (I) Kaplan–Meier curves indicating the percentage of mice with abnormally increased epileptiform activity relative to their own baseline at different days after the kainate injection. $p < 0.05$ by Mantel-Cox logrank test. $n = 15$ mice per group at the start of the experiment. Tick marks indicate mice euthanized for reasons unrelated to the experiment. Two-way ANOVA of the data in (C) revealed a significant effect of genotype ($p < 0.001$) and treatment ($p < 0.001$) and a significant interaction between them ($p < 0.001$). Dots in (C, E, F, and H) represent individual mice. *$p < 0.05$, **$p < 0.01$, ***$p < 0.001$ vs similarly treated WT mice or as indicated by the bracket, based on two-way ANOVA and Holm-Sidak test (C) or unpaired, two-tailed Student's t test (E, F, and H). Values in (C–H) are means ± s.e.m.

microglia for further activation by aberrant neural network activity. This hypothesis is supported by our finding that some of the gene expression changes (e.g., in *C1qa*, *Trem2*, and *Tyrobp*) were detected in the hippocampus but not cortex of 9-month-old mice, an age at which hAPP-J20 mice show prominent epileptiform activity and hippocampal amyloid plaques, but only sparse Aβ deposits in the cortex (Johnson et al., 2020). Furthermore, our *in situ* hybridization experiments showed that these gene expression changes in hAPP-J20 mice were most prominent in microglia/macrophages associated with plaques.

Since the main target of LEV is the synaptic vesicle glycoprotein 2A (Löscher et al., 2016) and we did not observe any direct effects of LEV on microglia in primary cultures lacking neurons, we find it most plausible to hypothesize that the effects of LEV on inflammation-related gene expression *in vivo* were mediated indirectly through changes in neuronal activities that affect microglia/macrophages and possibly also other types of glia. However, we cannot exclude that LEV affects genes, morphological parameters or functions of microglia/macrophages that we did not measure. LEV has been shown to affect some properties of immortalized microglial cell lines (Shima et al., 2018; Itoh et al., 2019), although it should be noted that such cell lines differ from primary microglia in many respects, including in their responses to LPS stimulation (Butovsky et al., 2014; Das et al., 2016). For the following reasons we also consider it most likely that the effects of tau reduction on inflammation-related gene expression resulted indirectly from the modulation of neuronal activities. Several lines of evidence suggest that tau reduction alters neuronal activities in ways that counteract hypersynchronous network activity (Chang et al., 2021), a type of network dysfunction that is known to change microglial activities (Eyo et al., 2017). Furthermore, neurons have robust levels of tau, whereas microglia and astrocytes express only minimal amounts of this gene product (Zhang et al., 2014; Saunders et al., 2018). However, because some oligodendrocytes express relatively high levels of tau (Zhang et al., 2014; Saunders et al., 2018), it is conceivable that tau reduction modulates interactions between oligodendrocytes and microglia, an intriguing possibility that deserves to be explored in future studies.

In general, inflammatory responses can be protective, harmful, or both (Wyss-Coray and Mucke, 2002; Meyer-Luehmann and Prinz, 2015; Sarlus and Heneka, 2017; Schartz and Tenner, 2020; Leng and Edison, 2021). It is likely that the inflammation-related gene expression changes we identified in hAPP-J20 mice enable adaptive, maladaptive, and innocent bystander responses by microglia and, possibly, other brain cells or blood-derived immune cells. In the current study, we began to dissect this range of possibility in relation to TREM2. We focused on TREM2 for four main reasons: (1) It is expressed in microglia/macrophages (refs (Efthymiou and Goate, 2017; Gratuze et al., 2018; Ulland and Colonna, 2018) and current study), (2) genetic alterations that impair the function of TREM2 strongly increase AD risk (Guerreiro et al., 2013; Jonsson et al., 2013; Efthymiou and Goate, 2017), (3) TREM2 expression was robustly increased in brain tissues of hAPP-J20 mice, and (4) this increase in TREM2 expression was effectively blocked by suppressing epileptiform activity with LEV treatment or tau ablation. Our finding that genetic reduction of TREM2 expression enhanced both spontaneous and kainate-induced epileptiform activity strongly suggests that the increased expression of TREM2 in hAPP mice represents an adaptive microglial response to the epileptiform activity in these mice. The same may be true for TYROBP, a TREM2-related gene product whose increased expression in hAPP-J20 mice was also reduced by LEV treatment and tau ablation.

Taken together, these findings indicate that TREM2 critically contributes to microglial functions that counteract hypersynchronous network activity and, perhaps, other types of network dysfunction. They are in line with other studies implicating microglia in the regulation of neuronal activities and the suppression of epileptic network activity (Li et al., 2012; Eyo et al., 2014, 2016; Szalay et al., 2016; Badimon et al., 2020; Umpierre and Wu, 2020; Merlini et al., 2021). Reduced levels or hypofunction of TREM2 would be expected to increase network dysfunction, particularly under conditions that promote network hypersynchrony, such as pathologically elevated levels of hAPP metabolites or microinfarcts, which are common in AD (Corrada et al., 2016) and could lead to intermittent excitotoxicity. Microglia with reduced or deficient TREM2 may be less able to curtail aberrant neuronal activities, which could increase amyloid formation (Cirrito et al., 2005; Bero et al., 2011; Yuan and Grutzendler, 2016) and the spread of abnormal tau species (Pooler et al., 2013; Yamada et al., 2014; Wu et al., 2016). Thus, in addition to previously identified possibilities (Gratuze et al., 2018; Ulland and Colonna, 2018; Hammond et al., 2019), run-away network dysfunction is a potential mechanism by which TREM2 hypofunction may promote the development of AD. Possibly consistent with this notion, Nasu-Hakola disease, a rare genetic disorder due to complete loss of TREM2 or TYROBP function, typically causes both epilepsy and dementia (Dardiotis et al., 2017).

Although several genome-wide association studies indicate that alterations in immune-related genes contribute to AD pathogenesis, the relevant variants are rare, including those of TREM2 (Guerreiro et al., 2013; Jonsson et al., 2013; Efthymiou and Goate, 2017). The mediators that lead from disease triggers to immune dysfunction in the most common, sporadic forms of AD remain to be unraveled. Our study suggests that aberrant neuronal activity—and in particular subclinical epileptiform activity, which occurs in a substantive proportion of sporadic AD cases (Vossel et al., 2016)—could be such a mediator.

Notably, tau reduction and LEV effectively reduced network dysfunction and aberrant microglial gene expression in the presence of high hAPP/Aβ levels in old brains. These interventions might be particularly beneficial when microglia have been rendered dysfunctional by disease, as they appear to suppress aberrant neural network activity (refs. (Li et al., 2012; Eyo et al., 2014; Eyo et al., 2016; Szalay et al., 2016; Badimon et al., 2020; Umpierre and Wu, 2020; Merlini et al., 2021) and this study). Because tau reduction and LEV prevented or reversed changes in the expression of diverse inflammation-related genes, these strategies might also reduce maladaptive and pathogenic immune responses. Their effects on hAPP/Aβ-induced C1Q elevation could be a case in point, as C1Q is also increased in AD brains (Tenner et al., 2018; Schartz and Tenner, 2020) and blocking C1Q with an antibody prevents synapse loss in hAPP mice (Hong et al., 2016; Tenner et al., 2018; Schartz and Tenner, 2020) and inhibits the development of epilepsy after traumatic brain injury (Holden et al., 2021).

Limitations of the study

Our molecular profiling focused on a circumscribed set of inflammation-related transcripts and on bulk tissue from specific brain regions. It would be interesting to expand this analysis to a single-cell analysis of all genes expressed in the brain across different regions. Many biological processes are not reflected in mRNA changes because they strictly occur at the levels of proteins, lipids, and other factors. It could, therefore, be informative to extend our transcriptomics analysis to other 'omics platforms. A limitation of most, if not all, of such studies is the inability to differentiate among adaptive, maladaptive and innocent bystander effects, an issue we addressed in regard to one of our lead hits by assessing the consequences of genetic TREM2 reduction in kainate-challenged mice. Because determining the sequence in which molecular alterations emerge can also help differentiate between causes and consequences, it could be useful to measure gene expression changes at additional ages. Experimental models simulate key aspects of a process or condition but rarely, if ever, recapitulate its full complexity. This is especially true for models of diseases as multifactorial and heterogeneous as AD. We previously validated various discoveries originally made in hAPP-J20 mice in both *App* knockin mice that do not overexpress APP (Orr et al., 2018; Johnson et al., 2020) and in humans with AD (Palop et al., 2003; Meilandt et al., 2008; Sanchez-Mejia et al., 2008; Verret et al., 2012; Vossel et al., 2013, 2016; Orr et al., 2015; Merlini et al., 2019). However, the hAPP-J20 model was developed to evaluate the specific pathogenic impact of FAD-mutant hAPP and, thus, does not include some other hallmarks of AD (e.g., neurofibrillary tangles). In general, it is difficult to predict whether the efficacy of therapeutic interventions observed in models designed to dissect rather than simulate the complexity of a disease will extrapolate to the human condition. It will, therefore, be important to assess the impact of LEV treatment and tau reduction also in alternate models designed to simulate the combined effects of multiple AD-related pathogenic factors. In a similar vein, while we simulated the hypofunction of *TREM2* variants that increase AD risk by genetic deletion of one *Trem2* allele in mice, it would be interesting to determine if expression of the actual human *TREM2* variants has similar effects. Notwithstanding these caveats, our study clearly highlights that the relationship between neural network activities and microglial functions in health and disease merits further investigation and so does the extent to which reducing network dysfunctions can prevent or halt the immunopathology and clinical manifestations of AD.

STAR★METHODS

Detailed methods are provided in the online version of this paper and include the following:

- KEY RESOURCES TABLE
- RESOURCE AVAILABILITY
  - Lead contact
  - Materials availability
  - Data and code availability
- EXPERIMENTAL MODEL AND SUBJECT DETAILS
  - Mice

SUPPLEMENTAL INFORMATION

Supplemental information can be found online at https://doi.org/10.1016/j.isci.2021.103245.

ACKNOWLEDGMENTS

We thank R. Thomas from Gladstone's Bioinformatics Core for helpful discussions, Gladstone's Behavioral Core for technical assistance, S. Ordway for editorial review, and R. Mott and E. Kimball for administrative assistance. This work was supported by United States National Institutes of Health grants RF1AG063519 and UH3AG054304 to L.M. and RR128928 to the Gladstone Institutes; a fellowship award from the Alzheimer's Association and an Alan Kaganov Scholarship to M.D.; and a gift from the Ray and Dagmar Dolby Family Fund to L.M.

AUTHOR CONTRIBUTIONS

M.D. and L.M. conceived and designed the study. M.D., W.M., E.S., S.T., G.Y., X.Y., K.H., X.W., and J.W. performed experiments. M.D., W.M., E.S., and L.M. analyzed the data. M.D. and L.M. wrote the paper with input from all coauthors.

DECLARATION OF INTERESTS

L.M. has received research funding from Cure Network Dolby Acceleration Partners (CNDAP) and has served on CNDAP's board of managers. He has also served on the scientific advisory boards of Arvinas, Biogen, and Dolby Family Ventures and has consulted for Eisai and Sangamo Therapeutics. L.M. is a coinventor on patents held by the Gladstone Institutes that focus on tau reduction as a strategy to block neural network dysfunction.

Received: August 20, 2021
Revised: September 27, 2021
Accepted: October 5, 2021
Published: November 19, 2021

REFERENCES

Alzheimer's Association (2020). 2020 Alzheimer's disease facts and figures. Alzheimers Dement *16*, 391–460. https://doi.org/10.1002/alz.12068.

Andoh, M., Ikegaya, Y., and Koyama, R. (2019). Synaptic pruning by microglia in epilepsy. J. Clin. Med. *8*, 1–16. https://doi.org/10.3390/jcm8122170.

Badimon, A., Strasburger, H.J., Ayata, P., Chen, X., Nair, A., Ikegami, A., Hwang, P., Chan, A.T., Graves, S.M., Uweru, J.O., et al. (2020). Negative feedback control of neuronal activity by microglia. Nature *586*, 417–423. https://doi.org/10.1038/s41586-020-2777-8.

Bakker, A., Krauss, G.L., Albert, M.S., Speck, C.L., Jones, L.R., Stark, C.E., Yassa, M.A., Bassett, S.S., Shelton, A.L., and Gallagher, M. (2012). Reduction of hippocampal hyperactivity improves cognition in amnestic mild cognitive impairment. Neuron *74*, 467–474. https://doi.org/10.1016/j.neuron.2012.03.023.

Bakker, A., Albert, M.S., Krauss, G., Speck, C.L., and Gallagher, M. (2015). Response of the medial temporal lobe network in amnestic mild cognitive impairment to therapeutic intervention assessed by fMRI and memory task performance. Neuroimage Clin. *7*, 688–698. https://doi.org/10.1016/j.nicl.2015.02.009.

Benjamini, Y., and Yekutieli, D. (2001). The control of the false discovery rate in multiple testing under dependency. Ann. Stat. *29*, 1165–1188. https://doi.org/10.1214/aos/1013699998.

Bero, A.W., Yan, P., Roh, J.H., Cirrito, J.R., Stewart, F.R., Raichle, M.E., Lee, J.M., and Holtzman, D.M. (2011). Neuronal activity regulates the regional vulnerability to amyloid-beta deposition. Nat. Neurosci. *14*, 750–756. https://doi.org/10.1038/nn.2801.

Bolte, S., and Cordelieres, F.P. (2006). A guided tour into subcellular colocalization analysis in light microscopy. J. Microsc. *224*, 213–232. https://doi.org/10.1111/j.1365-2818.2006.01706.x.

Butovsky, O., Jedrychowski, M.P., Moore, C.S., Cialic, R., Lanser, A.J., Gabriely, G., Koeglsperger, T., Dake, B., Wu, P.M., Doykan, C.E., et al. (2014). Identification of a unique TGF-beta-dependent molecular and functional

signature in microglia. Nat. Neurosci. *17*, 131–143. https://doi.org/10.1038/nn.3599.

Chang, C.W., Shao, E., and Mucke, L. (2021). Tau: enabler of diverse brain disorders and target of rapidly evolving therapeutic strategies. Science *371*, eabb8255. https://doi.org/10.1126/science.abb8255.

Cheng-Hathaway, P.J., Reed-Geaghan, E.G., Jay, T.R., Casali, B.T., Bemiller, S.M., Puntambekar, S.S., Von Saucken, V.E., Williams, R.Y., Karlo, J.C., Moutinho, M., et al. (2018). The Trem2 R47H variant confers loss-of-function-like phenotypes in Alzheimer's disease. Mol. Neurodegener. *13*, 1–12. https://doi.org/10.1186/s13024-018-0262-8.

Cirrito, J.R., Yamada, K.A., Finn, M.B., Sloviter, R.S., Bales, K.R., May, P.C., Schoepp, D.D., Paul, S.M., Mennerick, S., and Holtzman, D.M. (2005). Synaptic activity regulates interstitial fluid amyloid-b levels in vivo. Neuron *48*, 913–922. https://doi.org/10.1016/j.neuron.2005.10.028.

Corrada, M.M., Sonnen, J.A., Kim, R.C., and Kawas, C.H. (2016). Microinfarcts are common and strongly related to dementia in the oldest-old: the 90+ study. Alzheimers Dement. *12*, 900–908. https://doi.org/10.1016/j.jalz.2016.04.006.

Dardiotis, E., Siokas, V., Pantazi, E., Dardioti, M., Rikos, D., Xiromerisiou, G., Markou, A., Papadimitriou, D., Speletas, M., and Hadjigeorgiou, G.M. (2017). A novel mutation in TREM2 gene causing Nasu-Hakola disease and review of the literature. Neurobiol.Aging *53*, 194.e13–194.e22. https://doi.org/10.1016/j.neurobiolaging.2017.01.015.

Das, A., Kim, S.H., Arifuzzaman, S., Yoon, T., Chai, J.C., Lee, Y.S., Park, K.S., Jung, K.H., and Chai, Y.G. (2016). Transcriptome sequencing reveals that LPS-triggered transcriptional responses in established microglia BV2 cell lines are poorly representative of primary microglia. J. Neuroinflamm. *13*, 1–18. https://doi.org/10.1186/s12974-016-0644-1.

Efthymiou, A.G., and Goate, A.M. (2017). Late onset Alzheimer's disease genetics implicates microglial pathways in disease risk. Mol. Neurodegener. *12*, 1–12. https://doi.org/10.1186/s13024-017-0184-x.

El-Hayek, Y.H., Wiley, R.E., Khoury, C.P., Daya, R.P., Ballard, C., Evans, A.R., Karran, M., Molinuevo, J.L., Norton, M., and Atri, A. (2019). Tip of the iceberg: assessing the global socioeconomic costs of Alzheimer's disease and related dementias and strategic implications for stakeholders. J. Alzheimers Dis. *70*, 323–341. https://doi.org/10.3233/JAD-190426.

Eyo, U.B., Peng, J., Swiatkowski, P., Mukherjee, A., Bispo, A., and Wu, L.J. (2014). Neuronal hyperactivity recruits microglial processes via neuronal NMDA receptors and microglial P2Y12 receptors after status epilepticus. J. Neurosci. *34*, 10528–10540. https://doi.org/10.1523/JNEUROSCI.0416-14.2014.

Eyo, U.B., Peng, J., Murugan, M., Mo, M., Lalani, A., Xie, P., Xu, P., Margolis, D.J., and Wu, L.J. (2016). Regulation of physical microglia-neuron interactions by Fractalkine signaling after status epilepticus. eNeuro *3*, 1–14. https://doi.org/10.1523/ENEURO.0209-16.2016.

Eyo, U.B., Murugan, M., and Wu, L.J. (2017). Microglia-neuron communication in epilepsy. Glia *65*, 5–18. https://doi.org/10.1002/glia.23006.

Flaris, N.A., Densmore, T.L., Molleston, M.C., and Hickey, W.F. (1993). Characterization of microglia and macrophages in the central nervous system of rats: definition of the differential expression of molecules using standard and novel monoclonal antibodies in the normal CNS and in four models of parenchymal reaction. Glia *7*, 34–40. https://doi.org/10.1002/glia.440070108.

Fu, C.H., Iascone, D.M., Petrof, I., Hazra, A., Zhang, X., Pyfer, M.S., Tosi, U., Corbett, B.F., Cai, J., Lee, J., et al. (2019). Early seizure activity accelerates depletion of hippocampal neural stem cells and impairs spatial discrimination in an Alzheimer's disease model. Cell Rep. *27*, 3741–3751.e4. https://doi.org/10.1016/j.celrep.2019.05.101.

Garza, K.M., Zhang, L., Borron, B., Wood, L.B., and Singer, A.C. (2020). Gamma visual stimulation induces a neuroimmune signaling profile distinct from acute neuroinflammation. J. Neurosci. *40*, 1211–1225. https://doi.org/10.1523/JNEUROSCI.1511-19.2019.

GBD 2016 Dementia Collaborators (2019). Global, regional, and national burden of Alzheimer's disease and other dementias, 1990–2016: a systematic analysis for the Global Burden of Disease Study 2016. Lancet Neurol. *18*, 88–106. https://doi.org/10.1016/S1474-4422(18)30403-4.

Ghatak, A., and Combs, C.K. (2014). Iba1 immunoreactivity is enhanced following an antigen retrieval treatment with EDTA, pH 6.0. MethodsX *1*, 269–274. https://doi.org/10.1016/j.mex.2014.10.007.

Gratuze, M., Leyns, C.E.G., and Holtzman, D.M. (2018). New insights into the role of TREM2 in Alzheimer's disease. Mol. Neurodegener. *13*, 1–16. https://doi.org/10.1186/s13024-018-0298-9.

Guerreiro, R., Wojtas, A., Bras, J., Carrasquillo, M., Rogaeva, E., Majounie, E., Cruchaga, C., Sassi, C., Kauwe, J.S., Younkin, S., et al. (2013). TREM2 variants in Alzheimer's disease. N. Engl. J. Med. *368*, 117–127. https://doi.org/10.1056/NEJMoa1211851.

Gulbranson, D.R., Ho, K., Yu, G.Q., Yu, X., Das, M., Shao, E., Kim, D., Zhang, W.J., Choudhary, K., Thomas, R., et al. (2021). Phenotypic differences between the Alzheimer's disease-related hAPP-J20 model and heterozygous Zbtb20 knockout mice. eNeuro *8*, 1–21. https://doi.org/10.1523/ENEURO.0089-21.2021.

Hammond, T.R., Marsh, S.E., and Stevens, B. (2019). Immune signaling in neurodegeneration. Immunity *50*, 955–974. https://doi.org/10.1016/j.immuni.2019.03.016.

Harris, S.S., Wolf, F., De Strooper, B., and Busche, M.A. (2020). Tipping the scales: peptide-dependent dysregulation of neural circuit dynamics in Alzheimer's disease. Neuron *107*, 417–435. https://doi.org/10.1016/j.neuron.2020.06.005.

Hector, A., and Brouillette, J. (2021). Hyperactivity induced by soluble amyloid-beta oligomers in the early stages of Alzheimer's disease. Front. Mol. Neurosci. *13*, 1–15. https://doi.org/10.3389/fnmol.2020.600084.

Holden, S.S., Grandi, F.C., Aboubakr, O., Higashikubo, B., Cho, F.S., Chang, A.H., Forero, A.O., Morningstar, A.R., Mathur, V., Kuhn, L.J., et al. (2021). Complement factor C1q mediates sleep spindle loss and epileptic spikes after mild brain injury. Science *373*, eabj2685. https://doi.org/10.1126/science.abj2685.

Hong, S., Beja-Glasser, V.F., Nfonoyim, B.M., Frouin, A., Li, S., Ramakrishnan, S., Merry, K.M., Shi, Q., Rosenthal, A., Barres, B.A., et al. (2016). Complement and microglia mediate early synapse loss in Alzheimer mouse models. Science *352*, 712–716. https://doi.org/10.1126/science.aad8373.

Horváth, A., Szucs, A., Barcs, G., and Kamondi, A. (2017). Sleep EEG detects epileptiform activity in Alzheimer's disease with high sensitivity. J. Alzheimers Dis. *56*, 1175–1183. https://doi.org/10.3233/JAD-160994.

Iaccarino, H.F., Singer, A.C., Martorell, A.J., Rudenko, A., Gao, F., Gillingham, T.Z., Mathys, H., Seo, J., Kritskiy, O., Abdurrob, F., et al. (2016). Gamma frequency entrainment attenuates amyloid load and modifies microglia. Nature *540*, 230–235. https://doi.org/10.1038/nature20587.

Itoh, K., Taniguchi, R., Matsuo, T., Oguro, A., Vogel, C.F.A., Yamazaki, T., and Ishihara, Y. (2019). Suppressive effects of levetiracetam on neuroinflammation and phagocytic microglia: a comparative study of levetiracetam, valproate and carbamazepine. Neurosci. Lett. *708*, 1–7. https://doi.org/10.1016/j.neulet.2019.134363.

Johnson, E.C.B., Ho, K., Yu, G.Q., Das, M., Sanchez, P.E., Biljana, D., Lopez, I., Yu, X., Gill, M., Zhang, W., et al. (2020). Behavioral and neural network abnormalities in human APP transgenic mice resemble those of App knock-in mice and are modulated by familial Alzheimer's disease mutations but not by inhibition of BACE1. Mol. Neurodegener. *15*, 1–26. https://doi.org/10.1186/s13024-020-00393-5.

Jonsson, T., Stefansson, H., Steinberg, S., Jonsdottir, I., Jonsson, P.V., Snaedal, J., Bjornsson, S., Huttenlocher, J., Levey, A.I., Lah, J.J., et al. (2013). Variant of TREM2 associated with the risk of Alzheimer's disease. N. Engl. J. Med. *368*, 107–116. https://doi.org/10.1056/NEJMoa1211103.

Keren-Shaul, H., Spinrad, A., Weiner, A., Matcovitch-Natan, O., Dvir-Szternfeld, R., Ulland, T.K., David, E., Baruch, K., Lara-Astaiso, D., Toth, B., et al. (2017). A unique microglia type associated with restricting development of Alzheimer's disease. Cell *169*, 1276–1290.e17. https://doi.org/10.1016/j.cell.2017.05.018.

Lam, A.D., and Noebels, J. (2020). Night watch on the Titanic: detecting early signs of epileptogenesis in Alzheimer disease. Epilepsy Curr. *20*, 369–374. https://doi.org/10.1177/1535759720964775.

Lam, A.D., Deck, G., Goldman, A., Eskandar, E.N., Noebels, J., and Cole, A.J. (2017). Silent hippocampal seizures and spikes identified by foramen ovale electrodes in Alzheimer's disease. Nat. Med. *23*, 678–680. https://doi.org/10.1038/nm.4330.

Lam, A.D., Sarkis, R.A., Pellerin, K.R., Jing, J., Dworetzky, B.A., Hoch, D.B., Jacobs, C.S., Lee, J.W., Weisholtz, D.S., Zepeda, R., et al. (2020). Association of epileptiform abnormalities and seizures in Alzheimer disease. Neurology *95*, e2259–e2270. https://doi.org/10.1212/WNL.0000000000010612.

Leek, J.T., and Storey, J.D. (2007). Capturing heterogeneity in gene expression studies by surrogate variable analysis. PLoS Genet. *3*, 1724–1735. https://doi.org/10.1371/journal.pgen.0030161.

Leng, F., and Edison, P. (2021). Neuroinflammation and microglial activation in Alzheimer disease: where do we go from here? Nat. Rev. Neurol. *17*, 157–172. https://doi.org/10.1038/s41582-020-00435-y.

Li, Y., Du, X.F., Liu, C.S., Wen, Z.L., and Du, J.L. (2012). Reciprocal regulation between resting microglial dynamics and neuronal activity in vivo. Dev. Cell *23*, 1189–1202. https://doi.org/10.1016/j.devcel.2012.10.027.

Löscher, W., Gillard, M., Sands, Z.A., Kaminski, R.M., and Klitgaard, H. (2016). Synaptic vesicle glycoprotein 2A ligands in the treatment of epilepsy and beyond. CNS Drugs *30*, 1055–1077. https://doi.org/10.1007/s40263-016-0384-x.

Manders, E.M.M., Verbeek, F.J., and Aten, J.A. (1993). Measurement of co-localization of objects in dual-colour confocal images. Microscopy *169*, 375–382. https://doi.org/10.1111/j.1365-2818.1993.tb03313.x.

Martorell, A.J., Paulson, A.L., Suk, H.J., Abdurrob, F., Drummond, G.T., Guan, W., Young, J.Z., Kim, D.N., Kritskiy, O., Barker, S.J., et al. (2019). Multi-sensory gamma stimulation ameliorates Alzheimer's-associated pathology and improves cognition. Cell *177*, 256–271.e22. https://doi.org/10.1016/j.cell.2019.02.014.

Meilandt, W.J., Yu, G.-Q., Chin, J., Roberson, E.D., Palop, J.J., Wu, T., Scearce-Levie, K., and Mucke, L. (2008). Enkephalin elevations contribute to neuronal and behavioral impairments in a transgenic mouse model of Alzheimer's disease. J. Neurosci. *28*, 5007–5017.

Merlini, M., Rafalski, V.A., Rios Coronado, P.E., Gill, T.M., Ellisman, M., Muthukumar, G., Subramanian, K.S., Ryu, J.K., Syme, C.A., Davalos, D., et al. (2019). Fibrinogen induces microglia-mediated spine elimination and cognitive impairment in an Alzheimer's disease model. Neuron *101*, 1099–1108. https://doi.org/10.1016/j.neuron.2019.01.014.

Merlini, M., Rafalski, V.A., Ma, K., Kim, K.Y., Bushong, E.A., Rios Coronado, P.E., Yan, Z., Mendiola, A.S., Sozmen, E.G., Ryu, J.K., et al. (2021). Microglial Gi-dependent dynamics regulate brain network hyperexcitability. Nat. Neurosci. *24*, 19–23. https://doi.org/10.1038/s41593-020-00756-7.

Meyer-Luehmann, M., and Prinz, M. (2015). Myeloid cells in Alzheimer's disease: culprits, victims or innocent bystanders? Trends Neurosci. *38*, 659–668. https://doi.org/10.1016/j.tins.2015.08.011.

Mucke, L., Masliah, E., Yu, G.-Q., Mallory, M., Rockenstein, E., Tatsuno, G., Hu, K., Kholodenko, D., Johnson-Wood, K., and Mcconlogue, L. (2000). High-level neuronal expression of $A\beta_{1-42}$ in wild-type human amyloid protein precursor transgenic mice: synaptotoxicity without plaque formation. J. Neurosci. *20*, 4050–4058. https://doi.org/10.1523/JNEUROSCI.20-11-04050.2000.

Nygaard, H.B., Kaufman, A.C., Sekine-Konno, T., Huh, L.L., Going, H., Feldman, S.J., Kostylev, M.A., and Strittmatter, S.M. (2015). Brivaracetam, but not ethosuximide, reverses memory impairments in an Alzheimer's disease mouse model. Alzheimer Res. Ther. *7*, 1–12. https://doi.org/10.1186/s13195-015-0110-9.

Orr, A.G., Hsiao, E.C., Wang, M.M., Ho, K., Kim, D.H., Wang, X., Guo, W., Kang, J., Yu, G.Q., Adame, A., et al. (2015). Astrocytic adenosine receptor A_{2A} and G_s-coupled signaling regulate memory. Nat. Neurosci. *18*, 423–434. https://doi.org/10.1038/nn.3930.

Orr, A.G., Lo, I., Schumacher, H., Ho, K., Gill, M., Guo, W., Kim, D.H., Knox, A., Saito, T., Saido, T.C., et al. (2018). Istradefylline reduces memory deficits in aging mice with amyloid pathology. Neurobiol. Dis. *110*, 29–36. https://doi.org/10.1016/j.nbd.2017.10.014.

Palop, J.J., and Mucke, L. (2016). Network abnormalities and interneuron dysfunction in Alzheimer disease. Nat. Rev. Neurosci. *17*, 777–792. https://doi.org/10.1038/nrn.2016.141.

Palop, J.J., Jones, B., Kekonius, L., Chin, J., Yu, G.Q., Raber, J., Masliah, E., and Mucke, L. (2003). Neuronal depletion of calcium-dependent proteins in the dentate gyrus is tightly linked to Alzheimer's disease-related cognitive deficits. Proc. Natl. Acad. Sci. U S A *100*, 9572–9577. https://doi.org/10.1073/pnas.1133381100.

Pooler, A.M., Phillips, E.C., Lau, D.H., Noble, W., and Hanger, D.P. (2013). Physiological release of endogenous tau is stimulated by neuronal activity. EMBO Rep. *14*, 389–394. https://doi.org/10.1038/embor.2013.15.

Pottier, C., Ravenscroft, T.A., Brown, P.H., Finch, N.A., Baker, M., Parsons, M., Asmann, Y.W., Ren, Y., Christopher, E., Levitch, D., et al. (2016). TYROBP genetic variants in early-onset Alzheimer's disease. Neurobiol.Aging *48*, 222.e9–222.e15. https://doi.org/10.1016/j.neurobiolaging.2016.07.028.

R Core Team (2014). R: A language and environment for statistical computing (Vienna, Austria: R Foundation for StatisticalComputing). http://www.R-project.org/.

Ritchie, M.E., Phipson, B., Wu, D., Hu, Y., Law, C.W., Shi, W., and Smyth, G.K. (2015). Limma powers differential expression analyses for RNA-sequencing and microarray studies. Nucleic Acids Res. *43*, 1–13. https://doi.org/10.1093/nar/gkv007.

Roberson, E.D., Scearce-Levie, K., Palop, J.J., Yan, F., Cheng, I.H., Wu, T., Gerstein, H., Yu, G.-Q., and Mucke, L. (2007). Reducing endogenous tau ameliorates amyloid β-induced deficits in an Alzheimer's disease mouse model. Science *316*, 750–754. https://doi.org/10.1126/science.1141736.

Roberson, E.D., Halabisky, B., Yoo, J.W., Yao, J., Chin, J., Yan, F., Wu, T., Hamto, P., Devidze, N., Yu, G.-Q., et al. (2011). Amyloid-β/Fyn-induced synaptic, network, and cognitive impairments depend on tau levels in multiple mouse models of Alzheimer's disease. J. Neurosci. *31*, 700–711. https://doi.org/10.1523/JNEUROSCI.4152-10.2011.

Sanchez, P.E., Zhu, L., Verret, L., Vossel, K.A., Orr, A.G., Cirrito, J.R., Devidze, N., Ho, K., Yu, G.-Q., Palop, J.J., et al. (2012). Levetiracetam suppresses neuronal network dysfunction and reverses synaptic and cognitive deficits in an Alzheimer's disease model. Proc. Natl. Acad. Sci. U S A *109*, E2895–E2903. https://doi.org/10.1073/pnas.1121081109.

Sanchez-Mejia, R.O., Newman, J.W., Toh, S., Yu, G.Q., Zhou, Y., Halabisky, B., Cisse, M., Scearce-Levie, K., Cheng, I.H., Gan, L., et al. (2008). Phospholipase A_2 reduction ameliorates cognitve deficits in mouse model of Alzheimer's disease. Nat. Neurosci. *11*, 1311–1318. https://doi.org/10.1038/nn.2213.

Sarlus, H., and Heneka, M.T. (2017). Microglia in Alzheimer's disease. J. Clin. Invest. *127*, 3240–3249. https://doi.org/10.1172/JCI90606.

Saunders, A., Macosko, E.Z., Wysoker, A., Goldman, M., Krienen, F.M., De Rivera, H., Bien, E., Baum, M., Bortolin, L., Wang, S., et al. (2018). Molecular diversity and specializations among the cells of the adult mouse brain. Cell *174*, 1015–1030.e16. https://doi.org/10.1016/j.cell.2018.07.028.

Schartz, N.D., and Tenner, A.J. (2020). The good, the bad, and the opportunities of the complement system in neurodegenerative disease. J. Neuroinflamm. *17*, 1–25. https://doi.org/10.1186/s12974-020-02024-8.

Schartz, N.D., Wyatt-Johnson, S.K., Price, L.R., Colin, S.A., and Brewster, A.L. (2018). Status epilepticus triggers long-lasting activation of complement C1q-C3 signaling in the hippocampus that correlates with seizure frequency in experimental epilepsy. Neurobiol. Dis. *109*, 163–173. https://doi.org/10.1016/j.nbd.2017.10.012.

Schindelin, J., Arganda-Carreras, I., Frise, E., Kaynig, V., Longair, M., Pietzsch, T., Preibisch, S., Rueden, C., Saalfeld, S., Schmid, B., et al. (2012). Fiji: an open-source platform for biological-image analysis. Nat. Methods *9*, 676–682. https://doi.org/10.1038/nmeth.2019.

Shannon, P., Markiel, A., Ozier, O., Baliga, N.S., Wang, J.T., Ramage, D., Amin, N., Schwikowski, B., and Ideker, T. (2003). Cytoscape: a software environment for integrated models of biomolecular interaction networks. Genome Res. *13*, 2498–2504. https://doi.org/10.1101/gr.1239303.

Shi, J.Q., Wang, B.R., Tian, Y.Y., Xu, J., Gao, L., Zhao, S.L., Jiang, T., Xie, H.G., and Zhang, Y.D. (2013). Antiepileptics topiramate and levetiracetam alleviate behavioral deficits and reduce neuropathology in APPswe/PS1dE9 transgenic mice. CNS Neurosci.Ther. *19*, 871–881. https://doi.org/10.1111/cns.12144.

Shima, T., Sakuma, H., Suzuki, T., Kohyama, K., Matsuoka, T., Hayashi, M., Okumura, A., and Shimizu, T. (2018). Effects of antiepileptic drugs on microglial properties. Epilepsy Seizure *10*, 22–32. https://doi.org/10.3805/eands.10.22.

Sousa, C., Golebiewska, A., Poovathingal, S.K., Kaoma, T., Pires-Afonso, Y., Martina, S., Coowar, D., Azuaje, F., Skupin, A., Balling, R., et al. (2018). Single-cell transcriptomics reveals distinct inflammation-induced microglia signatures. EMBO Rep. *19*, 1–17. https://doi.org/10.15252/embr.201846171.

Sudom, A., Talreja, S., Danao, J., Bragg, E., Kegel, R., Min, X., Richardson, J., Zhang, Z., Sharkov, N., Marcora, E., et al. (2018). Molecular basis for the loss-of-function effects of the Alzheimer's disease-associated R47H variant of the immune receptor TREM2. J. Biol. Chem. *293*, 12634–12646. https://doi.org/10.1074/jbc.RA118.002352.

Szalay, G., Martinecz, B., Lenart, N., Kornyei, Z., Orsolits, B., Judak, L., Csaszar, E., Fekete, R., West, B.L., Katona, G., et al. (2016). Microglia protect against brain injury and their selective elimination dysregulates neuronal network activity after stroke. Nat. Commun. *7*, 1–13. https://doi.org/10.1038/ncomms11499.

Szklarczyk, D., Gable, A.L., Lyon, D., Junge, A., Wyder, S., Huerta-Cepas, J., Simonovic, M., Doncheva, N.T., Morris, J.H., Bork, P., et al. (2019). STRING v11: protein–protein association networks with increased coverage, supporting functional discovery in genome-wide experimental datasets. Nucleic Acids Res. *47*, D607–D613. https://doi.org/10.1093/nar/gky1131.

Tenner, A.J., Stevens, B., and Woodruff, T.M. (2018). New tricks for an ancient system: physiological and pathological roles of complement in the CNS. Mol. Immunol. *102*, 3–13. https://doi.org/10.1016/j.molimm.2018.06.264.

Ulland, T.K., and Colonna, M. (2018). TREM2 - a key player in microglial biology and Alzheimer disease. Nat. Rev. Neurol. *14*, 667–675. https://doi.org/10.1038/s41582-018-0072-1.

Umpierre, A.D., and Wu, L.J. (2020). How microglia sense and regulate neuronal activity. Glia, 1–17. https://doi.org/10.1002/glia.23961.

Vandesompele, J., De Preter, K., Pattyn, F., Poppe, B., Van Roy, N., De Paepe, A., and Speleman, F. (2002). Accurate normalization of real-time quantitative RT-PCR data by geometric averaging of multiple internal control genes. Genome Biol. *3*, 1–12. https://doi.org/10.1186/gb-2002-3-7-research0034.

Verret, L., Mann, E.O., Hang, G.B., Barth, A.M., Cobos, I., Ho, K., Devidze, N., Masliah, E., Kreitzer, A.C., Mody, I., et al. (2012). Inhibitory interneuron deficit links altered network activity and cognitive dysfunction in Alzheimer model. Cell *149*, 708–721. https://doi.org/10.1016/j.cell.2012.02.046.

Vossel, K.A., Beagle, A.J., Rabinovici, G.D., Shu, H., Lee, S.E., Naasan, G., Hegde, M., Cornes, S.B., Henry, M.L., Nelson, A.B., et al. (2013). Seizures and epileptiform activity in the early stages of Alzheimer disease. JAMA Neurol. *70*, 1158–1166. https://doi.org/10.1001/jamaneurol.2013.136.

Vossel, K.A., Ranasinghe, K.G., Beagle, A.J., Mizuiri, D., Honma, S.M., Dowling, A.F., Darwish, S.M., Van Berlo, V., Barnes, D.E., Mantle, M., et al. (2016). Incidence and impact of subclinical epileptiform activity in Alzheimer's disease. Ann. Neurol. *80*, 858–870. https://doi.org/10.1002/ana.24794.

Whitesell, J.D., Buckley, A.R., Knox, J.E., Kuan, L., Graddis, N., Pelos, A., Mukora, A., Wakeman, W., Bohn, P., Ho, A., et al. (2019). Whole brain imaging reveals distinct spatial patterns of amyloid beta deposition in three mouse models of Alzheimer's disease. J. Comp. Neurol. *527*, 2122–2145. https://doi.org/10.1002/cne.24555.

Wimo, A., Guerchet, M., Ali, G.C., Wu, Y.T., Prina, A.M., Winblad, B., Jönsson, L., Liu, Z., and Prince, M. (2017). The worldwide costs of dementia 2015 and comparisons with 2010. Alzheimers Dement. *13*, 1–7. https://doi.org/10.1016/j.jalz.2016.07.150.

Wu, J.W., Hussaini, S.A., Bastille, I.M., Rodriguez, G.A., Mrejeru, A., Rilett, K., Sanders, D.W., Cook, C., Fu, H., Boonen, R.A., et al. (2016). Neuronal activity enhances tau propagation and tau pathology in vivo. Nat. Neurosci. *19*, 1085–1092. https://doi.org/10.1038/nn.4328.

Wyss-Coray, T., and Mucke, L. (2002). Inflammation in neurodegenerative disease –a double-edged sword. Neuron *35*, 419–432. https://doi.org/10.1016/S0896-6273(02)00794-8.

Yamada, K., Holth, J.K., Liao, F., Stewart, F.R., Mahan, T.E., Jiang, H., Cirrito, J.R., Patel, T.K., Hochgrafe, K., Mandelkow, E.M., et al. (2014). Neuronal activity regulates extracellular tau in vivo. J. Exp. Med. *211*, 387–393. https://doi.org/10.1084/jem.20131685.

Yuan, P., and Grutzendler, J. (2016). Attenuation of beta-amyloid deposition and neurotoxicity by chemogenetic modulation of neural activity. J. Neurosci. *36*, 632–641. https://doi.org/10.1523/JNEUROSCI.2531-15.2016.

Zhang, B., Gaiteri, C., Bodea, L.G., Wang, Z., Mcelwee, J., Podtelezhnikov, A.A., Zhang, C., Xie, T., Tran, L., Dobrin, R., et al. (2013). Integrated systems approach identifies genetic nodes and networks in late-onset Alzheimer's disease. Cell *153*, 707–720. https://doi.org/10.1016/j.cell.2013.03.030.

Zhang, Y., Chen, K., Sloan, S.A., Bennett, M.L., Scholze, A.R., O'keeffe, S., Phatnani, H.P., Guarnieri, P., Caneda, C., Ruderisch, N., et al. (2014). An RNA-sequencing transcriptome and splicing database of glia, neurons, and vascular cells of the cerebral cortex. J. Neurosci. *34*, 11929–11947. https://doi.org/10.1523/JNEUROSCI.1860-14.2014.

STAR★METHODS

KEY RESOURCES TABLE

REAGENT OR RESOURCE	SOURCE	IDENTIFIER
Antibodies		
Goat anti-rabbit IgG (H+L) cross-adsorbed secondary antibody, Alexa Fluor 594	Invitrogen	Cat#: A-11012; RRID: AB_2534116
Goat anti-rabbit IgG (H+L) cross-adsorbed secondary antibody, biotinylated	Vector Laboratories	Cat#: BA-1000-1.5
Goat anti-rabbit IgG (H+L), HRP	Abcam	Cat#: ab6721
Rabbit monoclonal anti-C1q	Abcam	Cat#: ab182451; RRID: AB_2732849
Rabbit polyclonal anti-Aβ (3D6)	ATCC/Cell Essentials	Cat#: PTA-5130
Rabbit polyclonal anti-IBA1	Wako	Cat#: 019-19741; RRID: AB_839504
Tyramide (Opal 620 fluorophore)	Akoya Biosciences	Cat#: FP1495001KT
Bacterial and Virus Strains		
Ultrapure LPS, E. coli0111:B4	InvivoGen	Cat#: tlrl-3pelps
Chemicals, Peptides, and Recombinant Proteins		
Kainate	Tocris	Cat#: 0222; CAS: 487-79-6
Levetiracetam	ZerenexMolecular	Cat#: ZX-CF007056; CAS: 102767-28-2
Thioflavin S	Sigma-Aldrich	Cat#: T1892; CAS: 1326-12-1
Critical Commercial Assays		
DAB substrate kit	Vector Laboratories	Cat#: SK-4100
nCounter Neuroinflammation Panel, Mouse	NanoString	Cat#: 115000237
RNAscope Multiplex Fluorescent Assay v2	ACDBio	Cat#: 323100
VECTASTAIN Elite ABC-HRP Kit	Vector Laboratories	Cat#: PK-6100
Deposited Data		
Raw and analyzed NanoString data	This study	Tables S1, S2, and S3
Experimental Models: Organisms/Strains		
Mouse: C57BL/6J	The Jackson Laboratory	JAX: #000664
Mouse: hAPP-J20 (B6.Cg-*Zbtb20*$^{Tg(PDGFB-APPSwind)20Lms}$/2Mmjax)	Maintained in-house but available from The Jackson Laboratory	JAX: #34836
Mouse: *Mapt*$^{-/-}$(B6.129X1-*Mapt*^{tm1Hnd}/J)	The Jackson Laboratory	JAX: #007251
Mouse: *Trem2*$^{-/-}$ (C57BL/6J-*Trem2*^{em2Adiuj}/J)	The Jackson Laboratory	JAX: #027197
Oligonucleotides		
Mm00479862_g1 (*Aif1*) TaqMan Gene Expression Assay, FAM-MGB	ThermoFisher Scientific	Cat#: 4351370
Mm00432142_m1 (*C1qa*) TaqMan Gene Expression Assay, FAM-MGB	ThermoFisher Scientific	Cat#: 4331182
Mm03047343_m1 (*Cd68*) TaqMan Gene Expression Assay, FAM-MGB	ThermoFisher Scientific	Cat#: 4351370
Mm01183349_m1 (*Clec7a*) TaqMan Gene Expression Assay, FAM-MGB	ThermoFisher Scientific	Cat#: 4351370
Mm99999915_g1 (*Gapdh*) TaqMan Gene Expression Assay, VIC-MGB_PL	ThermoFisher Scientific	Cat#: 4448486
Mm00434228_m1 (*Il1b*) TaqMan Gene Expression Assay, FAM-MGB	ThermoFisher Scientific	Cat#: 4351370
Mm00446190_m1 (*Il6*) TaqMan Gene Expression Assay, FAM-MGB	ThermoFisher Scientific	Cat#: 4351370
Mm04209424_g1 (*Trem2*) TaqMan Gene Expression Assay, FAM-MGB	ThermoFisher Scientific	Cat#: 4331182

(*Continued on next page*)

Continued

REAGENT OR RESOURCE	SOURCE	IDENTIFIER
Mm00449152_m1 (*Tyrobp*) TaqMan Gene Expression Assay, FAM-MGB	ThermoFisher Scientific	Cat#: 4351370
RNAscope probe Mm-*C1qa*	ACDBio	Cat#: 441221
RNAscope probe Mm-*Trem2*-C2	ACDBio	Cat#: 404111-C2
RNAscope probe Mm-*Tyrobp-C3*	ACDBio	Cat#: 408191-C3
Software and Algorithms		
Cytoscape	Shannon et al. (2003)	https://cytoscape.org RRID: SCR_00302
FIJI	Schindelin et al. (2012)	https://imagej.net/Fiji RRID: SCR_002285
Imaris	Bitplane	https://imaris.oxinst.com RRID: SCR_007370
JACoP (FIJI plugin)	Bolte and Cordelieres (2006)	https://imagejdocu.tudor.lu/doku.php?id=plugin:analysis:jacop_2.0:just_another_colocalization_plugin:start
LabChart Pro	ADInstruments	https://www.adinstruments.com
limma (R package)	Ritchie et al. (2015)	https://bioconductor.org/packages/release/bioc/html/limma.html RRID: SCR_010943
nSolver Analysis	NanoString	https://www.nanostring.com RRID: SCR_003420
R	R Core Team (2014)	https://www.R-project.org/ RRID: SCR_00195
sva (R package)	Leek and Storey (2007)	https://bioconductor.org/packages/release/bioc/html/sva.html RRID: SCR_002155
Other		
Levetiracetam formulated chow, gamma irradiated	Custom made by Bio-Serv	Cat#: S7282
Placebo chow, gamma irradiated	Bio-Serv	Cat#: S7265

RESOURCE AVAILABILITY

Lead contact

Further information and requests for resources and reagents should be directed to and will be fulfilled by the Lead Contact, Lennart Mucke (lennart.mucke@gladstone.ucsf.edu).

Materials availability

This study did not generate unique reagents.

Data and code availability

- Tables S1, S2, and S3 include all NanoString data generated in this study. All other data reported in this paper will be shared by the lead contact upon reasonable request.
- This paper does not report original code.
- Any additional information required to reanalyze the data reported in this paper is available from the Lead Contact upon reasonable request.

EXPERIMENTAL MODEL AND SUBJECT DETAILS

Mice

hAPP-J20 mice were generated in-house (Mucke et al., 2000). *Mapt*$^{-/-}$ mice (Stock #007251) and *Trem2*$^{-/-}$ mice (Stock #027197) were from The Jackson Laboratory. All mice were maintained on a C57BL/6J

background. Experimental and control groups were sex-balanced, matched for age and background strain, and generated by the following breeding schemes. hAPP-J20 mice and WT controls were generated by breeding male heterozygous hAPP-J20 mice with female WT mice. *Mapt*$^{+/+}$ and *Mapt*$^{-/-}$ mice that did or did not express hAPP were generated by first breeding male heterozygous hAPP-J20 mice of the *Mapt*$^{+/+}$ background with female *Mapt*$^{-/-}$ mice. Experimental and control groups were then generated with F1 breeders by crossing male hAPP-J20/*Mapt*$^{+/-}$ mice with female *Mapt*$^{+/-}$ mice. To generate *Trem2*$^{+/-}$ mice and WT controls, we first bred male *Trem2*$^{-/-}$ mice with female WT mice. Experimental and control groups were then generated with F1 breeders by crossing male or female *Trem2*$^{+/-}$ mice with WT mice. Not all mice compared in individual experiments had the same parents and were raised by the same dam at the same time (littermates). Mice were housed in sex-matched groups of up to 5 mice per cage and maintained on a 12-h light/dark cycle. Unless indicated otherwise, mice were fed a regular chow diet (PicoLab Rodent Diet 5053, TestDiet and provided with water *ad libitum*. At the end of experiments, mice were deeply anesthetized with an IP injection of Avertin (2,2,2-tribromomethanol, 250 mg/kg body weight) and perfused transcardially with 0.9% NaCl. For RNA analyses, hemibrains were snap frozen and stored at −80°C. For immunohistochemical analyses, hemibrains were fixed in 4% PFA for 48 h and stored in PBS with 0.1% sodium azide at 4°C. Mice with tumors, a body condition score ≤2, or serious injuries from fighting were excluded from analyses. All animal procedures were approved by the Institutional Animal Care and Use Committee of the University of California, San Francisco.

Drug treatments of mice

Some mice were fed a diet containing 2,000 mg LEV per kg chow (S7282, custom made by Bio-Serv). Based on average food consumption, their daily intake of LEV was estimated at ∼300 mg/kg body weight. Placebo controls were fed the same diet without LEV (S7265, Bio-Serv). LEV and placebo chow were gamma-irradiated to meet mouse husbandry requirements. At the end of the treatment period, plasma levels of LEV were determined in a randomly selected subset of LEV-treated mice (n = 12). Briefly, 20 μl of blood was taken from the left cardiac ventricle of anesthetized mice and placed on ice in EDTA-containing tubes (ThermoFisher Scientific). Blood samples were centrifuged for 10 min at 25°C and the plasma supernatant was stored at −80°C until analysis. Plasma concentrations of LEV were determined by Charles River using HPLC, tandem mass spectrometry and internal standards. Plasma LEV levels were comparable in WT mice and hAPP-J20 mice (4.63 ± 0.339 vs. 5.05 ± 0.430 μg/ml, means ± s.e.m., n = 5–7 mice/group, p = 0.486 by unpaired, two-tailed Student's t-test). Other mice were treated with LPS or kainate. Ultrapure LPS (InvivoGen, *E. coli*0111:B4) was dissolved in endotoxin-free water to a stock concentration of 5 mg/ml. Kainate (Millipore-Sigma) was dissolved in 0.9% saline to a stock concentration of 4 mg/ml. For IP injections, LPS and kainate were further diluted in sterile 0.9% saline. Doses are stated in the main text or figure legends.

Primary microglial cultures

Mixed glial cultures were prepared from WT mouse pups at postnatal day 0–1. Hippocampal and cortical tissues were microdissected and dissociated in papain (Worthington) by repeated pipetting. Cells were plated in Dulbecco's modified Eagle's medium (Life Technologies) with 10% fetal bovine serum and penicillin-streptomycin. Seven days after plating, flasks were agitated in an orbital shaker for 1 h and microglia were collected, counted and plated in Dulbecco's modified Eagle's medium containing 1% N-2 Supplement (Thermo Fisher Scientific). Treatments with LEV (Zerenex Molecular) and LPS (InvivoGen, *E. coli*0111:B4) were initiated 2 days later as described in the legend to Figure S2.

METHOD DETAILS

Electroencephalography (EEG)

Lightweight EEG plugs were constructed in-house by soldering four Teflon-coated silver wire electrodes (0.125 mm diameter) to a multichannel electrical connector. Mice were anesthetized with isoflurane, and the electrodes were implanted under the skull and over the left and right frontal cortex (+1 mm anteroposterior (AP) and ± 1 mm mediolateral (ML) relative to the bregma) and the left and right parietal cortex (−2 mm AP and ± 1.7 mm ML relative to the bregma). The left frontal cortex was used as the reference electrode. Mice were allowed to recover from surgery for at least 2 weeks before EEG recordings began. Digital EEG activity and videos of their locomotor activity were recorded with a PowerLab data acquisition system. All signals were acquired at a sampling rate of 2 kHz. EEG recordings were analyzed with LabChart 8 Pro software (ADInstruments). Individual epileptic spikes were detected automatically with a macro

written in LabChart. Deflections were identified as epileptiform spikes if their amplitude was ≥4-fold higher than the average baseline of the trace and the absolute value of the second derivative of the slope was $\geq 10^4$. EEG traces and videos were also evaluated by an investigator blinded to genotype and treatment of the mice. Spikes judged to have resulted from movements or other artifacts were removed before quantitative analyses.

Behavioral testing

Mice were group-housed between behavioral tests. The investigators were blinded to their genotype and treatment. Behavioral tests were administered during the day time. Testing arenas were cleaned with 70% alcohol between mice. *Open field*. Spontaneous activity in an open field was assessed in a clear plastic chamber (41 × 41 × 30 cm) with photobeam arrays that automatically detected horizontal (16 × 16 photobeams) and vertical (16 photobeams) movements (Flex-Field/Open Field Photobeam Activity System, San Diego Instruments). Mice were allowed to acclimate to the testing room under normal light for 1 h before testing. During testing, mice were placed in the center of a clear plastic chamber and allowed to explore the chamber for 15 min. *Active place avoidance*. The testing chamber consisted of a square rotating arena with a grid floor (81 × 81 cm; Bio-Signal Group Corp.). A smaller, clear plastic circular enclosure (40 cm in diameter) with a circular lid was placed on the center of the grid floor. The arena was surrounded by large distal spatial cues. A 60° wedge within the 40 cm arena was designated as the aversive zone and was maintained in a constant position relative to the spatial cues outside the arena. During the first day, a habituation trial was conducted in which the mice were placed inside the enclosure, the arena was rotated clockwise (1 RPM), and the mouse was allowed to freely explore for 10 min with the aversive zone stimulation deactivated. On training days 1–4, mice were placed inside the enclosure and allowed to freely explore the rotating arena for 10 min with the stimulus generator activated for foot shock delivery upon entry into the aversive zone. One 10-min trial was performed per day over the course of 4 consecutive training days. 48 hours later, mice were placed inside the enclosure and allowed to freely explore the arena for 10 min with the aversive zone stimulus deactivated (probe trial). A Tracker video tracking system (Bio-Signal Group Corp.) was used to determine when the mice were inside the aversive zone. Upon entry, a 0.2 mA shock was delivered for 500 ms and repeated every 1.5 s until the mice left the aversive zone. The behavior of mice was video recorded and analyzed with Tracker (Bio-Signal Group Corp., Acton, MA). To assess learning performance in the APA, the raw number of entries into the aversive zone were transformed into rank summary scores using the Excel PERCENTRANK function, which returns the rank of a value in a dataset as a percentage of the dataset. Rank summary scores were calculated for each mouse relative to the scores of all genotypes obtained in any given trial. One rank summary score was then calculated for each mouse by averaging all of its rank summary scores across all training trials.

NanoString neuroinflammation panel

Total RNA was extracted from mouse hippocampi with RNeasy kits (Qiagen) and treated with DNase. For transcriptomic analysis, 0.5 μg of total RNA per sample was hybridized and multiplexed to probes from the NanoString Neuroinflammation gene expression panel (770 neuroinflammation-related mouse genes). Probes were designed and synthesized by NanoString nCounter Technologies. The target–probe complexes were captured, imaged, and digitally counted on the nCounter platform (SPRINT multiplex).

qRT-PCR

RNA isolated from the cortex of mice was reverse-transcribed with TaqMan reverse transcription reagents according to the manufacturer's protocol. The resulting cDNA was analyzed by qPCR with an ABI Prism 7900 HT Sequence Detection System, TaqMan Gene Expression Master Mix, and TaqMan primers with reporter dyes. Levels of each target cDNA were detected using FAM dye. Target cDNA levels were calculated by the $2^{-\Delta\Delta C}{}_T$ method, using *Gapdh* cDNA levels in the same well (detected with VIC dye) as a reference, and expressed relative to the mean of control values.

Histopathology

Coronal sections of PFA-fixed hemibrains (30 μm in thickness) were prepared with a cryostat (analyses involving RNA *in situ* hybridization) or a freezing microtome (all others). For ThioS staining of amyloid plaques, sections were washed 3 times in PBST and incubated for 10 min in 50% ethanol and PBS containing filtered 0.0015% ThioS and washed 3 times in PBST. Sections were mounted and counterstained with TO-PRO-3 (1:5000; ThermoFisher Scientific) and cover-slipped with ProLong Diamond Antifade Mountant

(ThermoFisher Scientific). For immunostaining of Aβ deposits, sections were incubated with 3% hydrogen peroxide and 10% methanol in PBS for 15 min at room temperature to quench endogenous peroxidase activity, and blocked for 1 h in 10% normal donkey serum, 1% non-fat dry milk, 0.2% gelatin, and PBS containing 0.5% Triton-X 100. Sections were incubated with the 3D6 primary antibody (1:1000; ATCC/Cell Essentials) diluted in 3% normal donkey serum overnight at 4°C. Sections were then washed three times in PBS with 0.25% Triton-X 100, and incubated in biotinylated anti-rabbit secondary antibody (1:500; Vector Laboratories). Signals were enhanced and visualized with Elite ABC and 3,3′-diaminobenzidine (DAB) tetrahydrochloride kits (Vector Laboratories). For immunostaining of C1Q and IBA1, free-floating sections were rinsed in PBST followed by incubation in 10 mM EDTA (pH 6.0) at 100°C for 10 min for antigen retrieval (Ghatak and Combs, 2014). After rinsing sections twice in PBS, endogenous peroxidase activity was quenched with 3% hydrogen peroxide in PBS for 10 min followed by a 1-h incubation in blocking solution containing 10% normal goat serum in PBS and 0.1% BSA. Sections were incubated in primary antibodies against C1Q (1:500; Abcam) or IBA1 (1:1000; Wako) at 4°C overnight. Sections were then washed in PBST and incubated with anti-rabbit secondary antibody conjugated to Alexa-Fluor 594 (1:500; Invitrogen) for 1 h in the dark, followed by 3 washes in PBST. For immunostaining following RNA *in situ* hybridization, cryosections were first hybridized with the RNA probe of interest according to the RNAscope protocol specifications. Sections were then blocked in 10% normal goat serum for 1 h and then incubated with IBA1 primary antibody at 4°C overnight. The next day, sections were washed in PBST and incubated with anti-rabbit secondary antibody conjugated to horseradish peroxidase (1:500; Abcam) for 2 h, incubated with fluorophore-labeled tyramide (1:750; Akoya Biosciences) for 10 min to intensify the signal, washed 3 times in PBST, stained with ThioS as above, and counterstained with DAPI (1:10000; ThermoFisher Scientific). Slides were imaged with an Aperio VERSA automated slide scanner using a 10× objective (for sections labeled with 3D6, anti-C1Q, or ThioS) or with an Olympus FV3000 Laser Scanning Confocal Microscope using a 20× or 40× objective (for sections labeled with ThioS, anti-IBA1, and mRNA probes).

QUANTIFICATION AND STATISTICAL ANALYSIS

Approaches to ensure robust and unbiased data collection and statistical analysis

Investigators were blinded to the genotype and treatment of mice and cultures during data collection. Group sizes were estimated based on previous results from similar experiments and from pilot studies. Statistical analyses were done with Excel (v.16.46), Prism 8.0 (GraphPad) and R (v.3.6.2). The normality of data was assessed by D'Agostino and Pearson omnibus normality test or by Shapiro-Wilk test. Variances were compared by Bartlett's test or F-test. Differences between two groups were assessed by unpaired, two-tailed Student's *t*-test and differences among multiple groups by two-way ANOVA followed by Holm-Sidak post hoc test. Null hypotheses were rejected at the 0.05 level. Statistical details for each experiment can be found in the figure legends. Additional statistical information is described in the NanoString analyses section below.

NanoString analyses

Raw files were processed with nSolver Analysis v4.0 to normalize gene expression datasets by the geNORM method (Vandesompele et al., 2002) using the geometric mean of nine housekeeping genes. The NanoString panel also included six synthetic DNA positive control targets with known concentrations and eight negative control probes designed against engineered RNA sequences not present in biological samples. Transcripts with an expression value < 20 were excluded from analysis. Expression profiles of the remaining 621 transcripts were log-transformed and quantile-normalized before further analysis. The *limma* package in R v3.6.2 was applied to gene expression data for differential expression analysis (Ritchie et al., 2015). T-statistics for group comparisons were calculated with robust empirical Bayes methods. p values from t-statistics were adjusted for multiple comparisons by the Benjamini–Yeuketeli method (Benjamini and Yekutieli, 2001) and $p < 0.05$ was considered significant. For STRING analyses, gene expression changes were subjected to protein network analysis (Szklarczyk et al., 2019) using the STRING database v11.0 with a confidence score cutoff of 0.4 and allowing STRING to recommend three additional gene products of interest. The resulting protein-protein interaction networks were visualized with Cytoscape v3.7.2 (Shannon et al., 2003). To identify genes whose expression was modulated by LEV treatment and tau ablation in Figures 5K–5M, three independent groups of mice were combined in a linear model. To account for batch effects and potential hidden confounding variables, we performed a surrogate variable analysis on the expression data using the sva package in R (Leek and Storey, 2007). Estimated surrogate variables were included as covariates in the linear regression modeling analysis.

Immunohistochemical quantification and analyses

For the quantitative analysis of ThioS labeled plaques, three hemibrain sections per mouse were analyzed by FIJI (Schindelin et al., 2012). For each section, the region of interest was defined as the outer border of the hippocampus. ThioS positive deposits within the outlined region were thresholded and the Analyze Particles plugin was used to count the total number of plaques within the area of interest. The number of plaques in each section was divided by the area of the hippocampus. Plaques touching the border of the outline were not counted. For each plaque within the area of interest, the area occupied, circularity and mean grey values (the average pixel intensity within an area of interest) were recorded. For quantitative analysis of C1Q immunolabeled sections, three hemibrain sections per mouse were analyzed by FIJI. The area and mean grey values from the whole hippocampus were recorded. For the quantitative analysis of IBA1-and ThioS-labeled sections, three brain sections per mouse were analyzed by FIJI and Imaris. For each section, three plaques (circumference: 209 μm ± 1.24, mean ± s.e.m) were chosen for analysis. To calculate the number of microglia/macrophages surrounding plaques, the Spots tool in Imaris was used to identify the number of IBA1-positive cell bodies within 25 μm from the perimeter of each plaque. To calculate the fraction of fluorescent signal overlap between the IBA1 and ThioS channels, Mander's overlap coefficient (Manders et al., 1993) was calculated using the JACoP plugin in FIJI (Bolte and Cordelieres, 2006). To determine the effect of plaque distance on the soma size of microglia/macrophages, three IBA1-positive cell bodies located within 25 μm from the perimeter of a plaque and three IBA1-positive cell bodies located > 25 μm away from the nearest plaque were analyzed. Images were thresholded and the Analyze Particles plugin in FIJI was used to measure the average area and circularity of each cell body.